Annual layer counting in the Bølling-Allerød and Younger Dryas sections of the GRIP ice core using deconvoluted isotope data, dust and chemical data

Master thesis

by

Inger Kathrine Seierstad

Supervisor: Sigfús J. Johnsen
Ice and Climate Group
Faculty of Science
University of Copenhagen

25th June 2005

Contents

1 Abstract

A new dating of Bølling-Allerød (Greenland Interstadial 1) and Younger Dryas (Greenland Stadial 1) periods in the GRIP ice core is presented. Newly measured profiles of δD and δ^{18}O, as well as existing profiles of [Ca^{2+}], [NH_4^+], dust concentrations, [NO_3^-] and ECM have been used for the dating. As seasonal variations can be observed in all seven components, it has been possible to simultaneously count annual layers in the profiles in order to obtain a multi parameter dating.

The new data presented in this study includes a total of 22 m of δD profiles of 1 cm resolution from three sections of the Bølling-Allerød period in the GRIP ice core. The δD measurements have been performed on a Micromass SIRMS (Stable Isotope Ratio Mass Spectrometer), using a sample size of $\sim$0.5μl. The δD data have been corrected for minor drift and memory. The new δD data and two previously measured δ^{18}O series have been deconvoluted to correct for diffusion in the firn and ice.

The annual layer counting suggests a duration of the Bølling, Older Dryas, Allerød and Younger Dryas periods of 588$\pm$16, 70$\pm$4, 971$\pm$31 and 1150$\pm$44 years, respectively. Comparison with the new NGRIP stratigraphical dating (the GICC05 timescale) and with other stratigraphical and modelled time scales from Greenland ice cores, indicates that the presented durations should be considered as minimum estimates.

2 Acknowledgements

The author would like to thank Sigfús J. Johnsen for hours of inspiring and helpful supervision during the whole master project. I would also like to thank Bo M. Vinther for discussions about the MEM-method and for collaboration on some of the annual layer counting, Sune O. Rasmussen for providing the program Datetool that I have used extensively through this work and Trine Ebbensgaard Strømfeldt, Thore Jürgensen and Anita Boas for providing the high resolution δ^{18}O data. The staff at the AMS ^{14}C Dating Centre), Department of Physics and Astronomy, University of Århus, Denmark is also thanked for helpful assistance during the δD analysis; in special I am indebted to Jesper Olsen who taught me how to use the mass spectrometer and with whom I have had discussions about the δD data. During the writing process of the paper [Seierstad et al., In press] I got helpful review from Veijo Pohjola and an anonymous reviewer and also fruitful comments from the scientific editor, Elisabeth Isaksson. I would like to thank Statens Lånekasse For Utdanning, Copenhagen Ice Core Dating Initiative (funded by the Carlsberg Foundation), Dansk Geofysisk Forening and former Geofysisk Afdeling for financial support. Finally, I would like to thank Sune O. Rasmussen and Anders R. Kristensen for proof-reading.

3 Introduction

Along with the focus on global warming there has been an increased scientific, political and daily-life interest in understanding how the complex climate system of the Earth works. Information on the Earths' climate over time is recorded in terrestrial, marine and ice cores drilled in different regions of the world. By studying the so-called climate proxies from these archives a chronology of climatic events in the past can be established. A precise and high-resolution dating of the archives is important to be able to understand the mechanisms involved in climate changes and the relative timing of events observed in climate proxies at different locations. Also the different chronologies have to be linked through time-synchronous marker horizons (e.g. volcanic ash layers), so that possible leads and lags between different climatic sub-systems can be revealed. Ice cores from Greenland are ideal for high-precision dating of climatic events, as they are characterised by high time resolution, while still covering relatively long time spans back in time.

The 3028 m long GRIP (GReenland Ice Core Project) ice core from the Summit of the Greenland ice cap (Figure 3.1) constitutes a continuous archive of past accumulation, containing information of past climate in Greenland back to $\sim$120 ka BP [GRIP Members, 1993]. Results from the GRIP ice core confirmed earlier indications [Johnsen et al., 1972, 1992b] of the existence of periods of relatively mild climate, the so-called interstadials, in Greenland during the last glacial period [Johnsen et al., 1992a]. Abrupt climatic changes during the last glacial period have also been revealed in numerous marine and terrestrial archives showing that climatic oscillations were prevailing on a large scale [Bond et al., 1993]. The climatic oscillations during the last glacial are recorded in the oxygen isotope profile

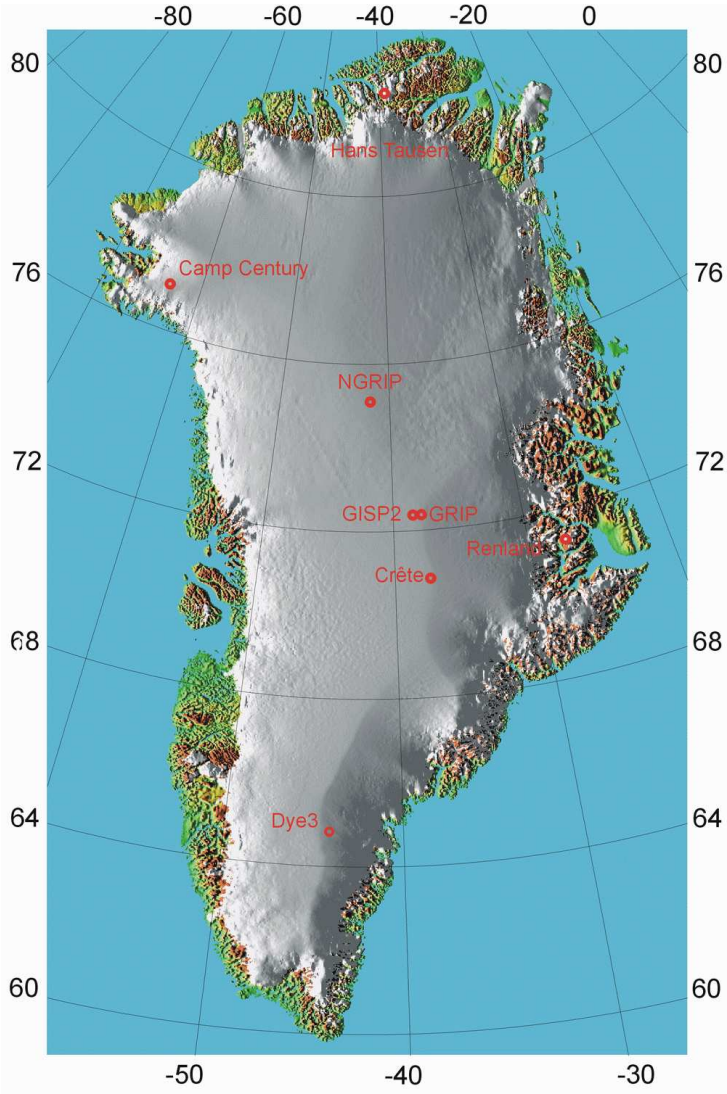

Figure 3.1: Deep ice cores drilled in Greenland. The GRIP (GReenland Ice Core Project) ice core was drilled in 1989-1992 at Summit (72 ° 34'N 37 ° 37'W) [GRIP Members, 1993]. The GISP2 (Greenland Ice Sheet Project Two) ice core is situated 28 km W of GRIP and the NGRIP (North GReenland Ice Core Project) ice core is located 325 km NW of GRIP [Grootes et al., 1993; Dahl-Jensen et al., 2002]. Map by S. Ekholm, Kort & Matrikelstyrelsen, Denmark.

from the GRIP core. The upper panel in Figure 3.2 displays the δ^{18}O from the GRIP ice core in 50 years averages, down to $\sim$50 ka BP [Johnsen et al., 2001]. The numbers refer to the numbering of the Greenland Interstadials, as suggested by [Johnsen et al., 1992a]. This study deals with ice from the relatively warm climate period Greenland Interstadial 1 (Bølling-Allerød) and the relatively cold Stadial 1 (Younger Dryas) at the end of the last glacial period. Accumulation deposited at, or close to the GRIP drill site within these two periods is found more than half way down through the ice sheet at present, each annual layer having a thickness of around 3-5 cm [Dahl-Jensen et al., 1993; Johnsen et al., 2001]. The bottom panel of Figure 3.2 zooms in on the Bølling-Allerød and Younger sections found at a depth of 1600-1700 m in the GRIP core.

Before presenting the exact objectives of this study, an introduction to the existing time scales for the GRIP core is needed. There exist modelled time scales of the GRIP ice core down to the Eemian at $\sim$120 ka BP [Johnsen et al., 2001] and a stratigraphical timescale down to 60 ka BP. The Holocene part of the stratigraphical dating of the GRIP ice core is based on annual layer counting using δ^{18}O, Electrical Conductivity Measurements (ECM), [Ca^{2+}] and [NH_4^+] profiles [Fuhrer et al., 1993, 1996; Johnsen et al., 1999]. Recently, Rasmussen et al. [Submitted] presented a new common stratigraphical timescale for the NGRIP and GRIP ice cores, covering the time interval 7.9-14.85 ka before A.D. 2000 (b2k), under the name Greenland Ice Core Chronology 2005 (GICC05). The new timescale includes a revised stratigraphical dating of the GRIP core in the interval 7.9-11.75 ka b2k (1299.81-1624.27m), i.e. from the so-called 8.2 ka event to the transition from Younger Dryas to Preboreal. The new interpretation of this section of the GRIP data draws on the experience obtained from annual layer counting using extensive high-resolution Continuous Flow Analysis (CFA) data, as well as ECM and visual stratigraphy data, from the NGRIP ice core. Before 11.75 ka b2k, i.e. in Younger Dryas and downwards through Bølling-Allerød the GICC05 timescale is based solely on NGRIP data.

Stratigraphical dating of glacial ice from Younger Dryas back to 60 ka BP in the

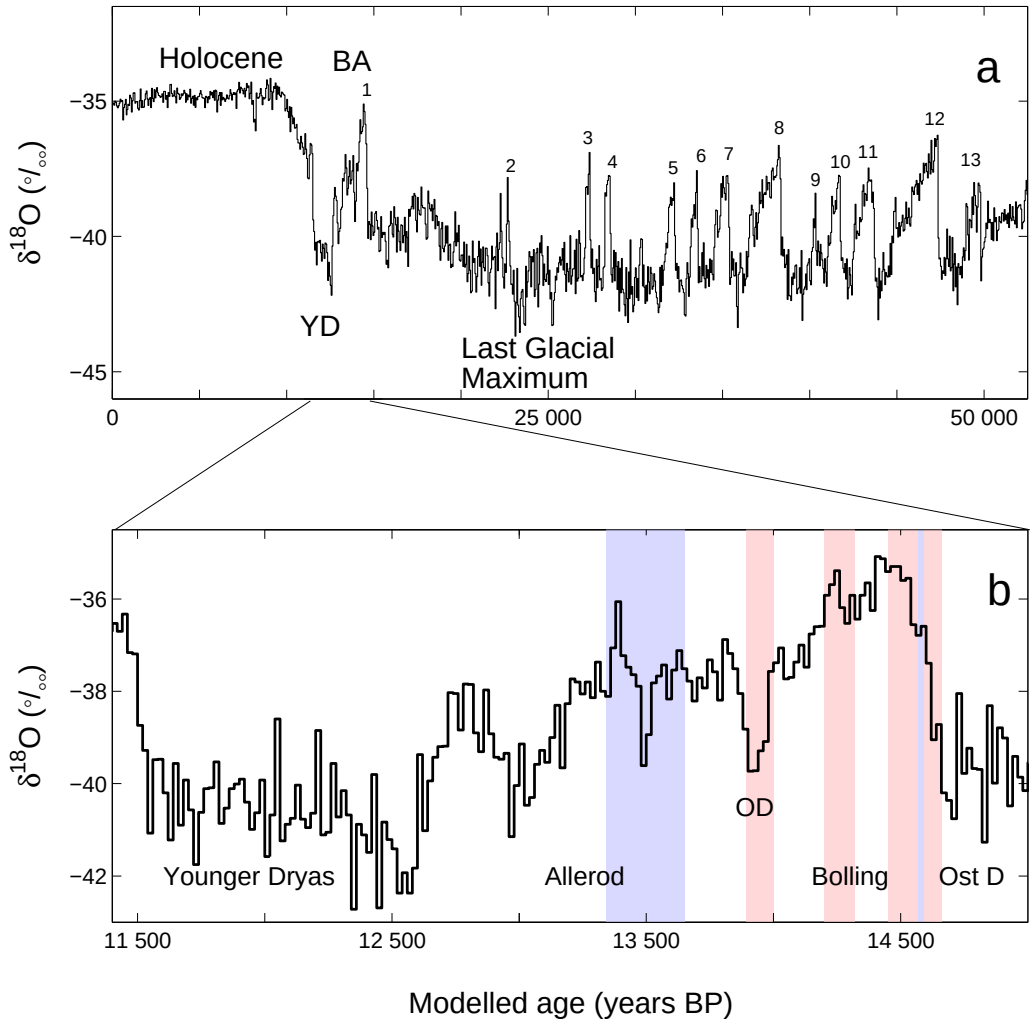

Figure 3.2: Bølling-Allerød and Younger Dryas. δ^{18}O-profiles on a modelled time scale (ss09sea), where BP=1990 [Johnsen et al., 2001]. (a) 50 year averages of δ^{18}O. Bølling-Allerød (BA) is the last interstadial (GI 1) before the cold Younger Dryas (YD, Stadial 1) and the subsequent warming in the Pre-Boreal at the start of Holocene. (b) Zoom of the interval which is subject to investigation. Data are 20 year averages of δ^{18}O. The three light red bands indicate the intervals, where ice has been sampled and analysed for δD in high resolution to retrieve annual layers and improve the dating of the climate period. The light blue areas show the intervals where detailed δ^{18}O has been included in the dating. Please note that the deepest δ^{18}O-series overlaps a 1.1 m section of the deepest δD-interval. See Table 6.1 for the depth intervals of the stable isotopes sections. OD and Ost D denote the periods known as Older Dryas and Oldest Dryas, respectively.

GRIP core is based on seasonal variations of dust concentrations only [Hammer et al., 1997; Hammer, In press; The Greenland Summit Ice cores CD-ROM, 1997]. As dust is brought to Greenland by storms, peaks in the dust records are, however, likely to represent depositional events, rather than annuality. Due to this, the dust record may show "double peaks" within one year, even though the ice core records in general contain about one dust peak per year. When having only this parameter for dating, there is therefore a risk of overestimating the number of years.

Motivated by this fact, this study was set up to include as many independent parameters as possible in the dating of Bølling-Allerød and Younger Dryas, all data series measured in high-resolution and showing seasonal variations. These data profiles include [Ca^{2+}] and [NH_4^+] [Fuhrer et al., 1993, 1996], dust and [NO_3^-] [Hammer et al., 1997; Hammer, In press] all existing over the whole period investigated, and new sections of δD and δ^{18}O data from certain intervals of the Bølling-Allerød section. The main focus has been on the stable isotope profiles within the Bølling-Allerød section, as these parameters are regarded to be the optimal parameters for dating ice cores under favourable conditions. They show a strong seasonal cycle, with high values during summer times and low values during winter times, and are thus closely linked to the seasonal signal without relying too much on individual precipitation events. However, diffusion of isotopes in the firn and ice leads to smoothening of the isotope profile as time goes by [Johnsen, 1977; Johnsen et al., 2000]. Hereby the annual cycle, which is of interest for annual layer counting, is weakened at greater depths. The diffusion process in the firn is dependent on temperature and annual accumulation rates. For the annual cycle to survive the densification process in Greenland the annual accumulation rate has to be greater than $\sim$0.2 m ice per year [Johnsen, 1977]. At present at the GRIP site, the accumulation rate is $\sim$ 0.23 m ice per year and the average annual temperature is -32 $^\circ$C [Johnsen et al., 1992a].
Until now, stable isotopes have not been used as a dating tool within the glacial period, partly because of low accumulation during glacial times, which means that the annual isotope signal is severely dampened, and partly because the thin

annual layers require a high sampling rate. The interstadial Bølling-Allerød was characterised by a relatively warmer climate and a higher accumulation rate compared to the rest of the glacial period [Johnsen et al., 1995], which is promising for retaining the annual cycle.

The aim of this study is to investigate if it is possible to retrieve the annual signal in isotope data from the Bølling-Allerød section in the GRIP core and, if so, to estimate the duration of this interstadial by counting annual cycles in high-resolution isotope data together with annual cycles recorded in available high-resolution series of ECM, $[Ca^{2+}]$, $[NH_4^+]$, $[NO_3^-]$ and dust concentration. For this purpose ice have been sampled in 1 cm resolution in three intervals, covering a total of 22 m, within the Bølling-Allerød period in the GRIP ice core, as illustrated in Figure 3.2. δD analysis have been performed on these samples on a stable isotope ratio mass spectrometer. Deconvolution techniques have been applied to the new δD series and two previously measured δ^{18}O series from Bølling-Allerød, aiming at detecting and amplifying the annual signal, which has been weakened by diffusion in the firn and ice.

Furthermore, another objective has been to include the Younger Dryas section of the GRIP core in the multi-parameter dating, aiming at filling the gap between the new Bølling-Allerød annual layer counting from this work and the GRIP part of the new GICC05 timescale [Rasmussen et al., Submitted].

Structure of the thesis

An introduction to stable hydrogen and oxygen isotopes in ice cores is given in *Chapter 4*. Here it is outlined how δD and δ^{18}O can be used for absolute dating of ice cores and how these profiles are influenced by diffusion in the firn and ice. A deconvolution technique, which has been applied to correct for the diffusion effect is presented. *Chapter 5* gives a thorough description of the experimental part of this project, which consists of δD analysis of ice samples from the Bølling-Allerød period in the GRIP ice core. The data processing of the hydrogen isotope data is presented in the last section of this chapter. A brief description of the

high resolution GRIP data that have been used in the multi-parameter dating of Bølling-Allerød and Younger Dryas is found in *Chapter 6*. The results from the diffusion correction of the stable isotopes are presented along with the presentation of the stable isotope data. *Chapter 7* is devoted to the dating part of this work. The applied annual layer counting method is outlined and the various steps in the dating process are described. The first results of the dating work, including estimates of the duration of the Bølling, Older Dryas and Allerød periods, were presented in [Seierstad et al., In press, see Appendix A]. In this chapter new and improved results on the dating are presented and discussed. This includes a detailed comparison of the results from this work with the new NGRIP annual layer counting (GICC05, Rasmussen et al. [Submitted]) and an estimate of the duration of Younger Dryas period in the GRIP core, based on multi-parameter annual layer counting. Finally *Chapter 8* summarises the main conclusions of this study. The *Appendix* includes the paper Seierstad et al. [In press]. Topics that are considered to be of limited interest for most readers, i.e. details upon the δD analysis, can be found in the appendix as well.

4 Stable isotopes in ice cores

The isotopic composition of snow deposited in polar regions reflects the temperature in the air mass at the time of snow deposition. This feature allows a reconstruction of past temperature changes from the information recorded in the stable isotope profiles [Dansgaard, 1964; Johnsen et al., 1995]. On shorter time scales the strong relationship between isotopic composition and temperature is reflected as seasonal variations in the stable isotope profiles. These seasonal cycles can be used for absolute dating of ice cores under favourable conditions [Epstein and Sharp, 1959; Benson, 1962; Dansgaard, 1964]. It is the latter application of stable isotope profiles that is of interest for this project.
The chapter starts with a presentation of how the isotopic ratios $^{18}O/^{16}O$ and D/H normally are reported, and how stable isotope records can be used for absolute dating of ice cores. The rest of the chapter deals with the effect of diffusion in firn and ice on the stable isotope profiles. The methods used for diffusion correction in this work are presented.

4.1 Definition of δD and δ^{18}O

The three most important isotopic components of natural water is $H_2^{16}O$, $H_2^{18}O$ and $HD^{16}O$. The isotopic composition of a water sample x is normally reported on the δ scale, as the relative difference in ‰ between the isotopic ratio of the sample (R_x) and the isotopic ratio of a standard (R_{Std}):

$$\delta_{x/Std} = \left(\frac{R_x - R_{Std}}{R_{Std}} \right) * 1000 \text{ ‰} \tag{4.1}$$

The isotopic ratio R is the concentration of the heavy isotope relative to the concentration of the light isotope, i.e. R= $\frac{[\mathrm{D}]}{[\mathrm{H}]}$ for δD and R= $\frac{[^{18}\mathrm{O}]}{[^{16}\mathrm{O}]}$ for δ^{18}O.

4.1.1 Normalisation to the VSMOW-SLAP scale

When measuring isotopic ratios $\frac{\mathrm{D}}{\mathrm{H}}$ and $\frac{^{18}\mathrm{O}}{^{16}\mathrm{O}}$ of a water sample x the results are normally reported relative to the international standard VSMOW (Vienna Standard Mean Ocean Water), which per definition has a δD and a δ^{18}O value of 0‰ [Craig, 1961]. The use of a standard, such as VSMOW, improves the accuracy of the measurements and it facilitates inter-laboratory comparison of results. However, the *difference* in measured values of two samples may vary from one mass spectrometer to another and from one operational setting to another. To work around this phenomenon of scale contraction (or expansion), another primary standard, SLAP (Standard Light Antarctic Precipitation), is used for normalisation purposes [IUPAC, 1994; Coplen, 1988]. This standard has by convention a δD and a δ^{18}O value of -428‰ and -55.5‰, respectively [Gonfiantini, 1978]. The normalisation is a process of stretching or shrinking the measured δ-scale so that the δ-value of SLAP corresponds to the accepted value relative to VSMOW.

During daily analysis the normalisation is usually done by using secondary standards (here called Std1 and Std2) instead of the primary standards VSMOW and SLAP. These secondary standards are measured along with the unknown samples in a run and they are periodically calibrated to VMSOW and SLAP. The actual calculations on the calibration and normalisation can be done in slightly different ways [Coplen, 1988; Nelson, 2000; Werner and Brand, 2001]. The following procedure has been applied on the δD samples in this project.
The raw values are given relative to a working standard (of an arbitrary value), here called reference gas (Ref). These raw values are expressed relative to VSMOW in a two-step process. First, all numbers are expressed relative to laboratory stan-

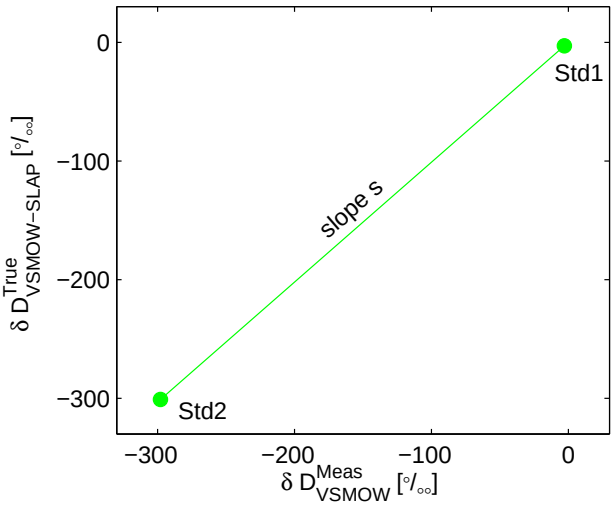

Figure 4.1: Normalisation to the VSMOW-SLAP scale is done by using the slope s of the linear regression between measured and accepted values of the secondary standards Std1 and Std2 as a scaling coeffi cient for unknown samples.

dard Std1 according to:

$$\delta \mathrm{D}_{x/Std1} = \delta \mathrm{D}_{x/Ref} + \delta \mathrm{D}_{Ref/Std1} + \frac{\delta \mathrm{D}_{x/Ref} \cdot \delta \mathrm{D}_{Ref/Std1}}{1000} \tag{4.2}$$

where

$$\delta \mathrm{D}_{Ref/Std1} = \left(\frac{1000}{\delta \mathrm{D}_{Std1/Ref} + 1000} - 1 \right) \cdot 1000$$

Now, calibration to the VSMOW scale can be performed by using Equation 4.2 again, where the former output has become input:

$$\delta \mathrm{D}_{x/VSMOW} = \delta \mathrm{D}_{x/Std1} + \delta \mathrm{D}_{Std1/VSMOW} + \frac{\delta \mathrm{D}_{x/Std1} \cdot \delta \mathrm{D}_{Std1/VSMOW}}{1000} \tag{4.3}$$

where $\delta \mathrm{D}_{Std1/VSMOW}$ is the accepted value of the secondary standard Std1. The normalisation is now performed by plotting the values of the laboratory standards as illustrated in Figure 4.1 and making a linear regression. The slope s of the re-

sulting equation is used as a scaling coefficient to normalise the measured values:

$$s = \frac{\delta \mathrm{D}^{True}_{Std1/VSMOW-SLAP} - \delta \mathrm{D}^{True}_{Std2/VSMOW-SLAP}}{\delta \mathrm{D}^{Meas}_{Std1/VSMOW} - \delta \mathrm{D}^{Meas}_{Std2/VSMOW}} \tag{4.4}$$

The scaling coefficient s is the ratio of the accepted and the measured differences between the two standards. If $s > 1$ the isotopic scale of the mass spectrometer is contracted relative to the VSMOW-SLAP scale, while a normalisation constant less than 1 corresponds to an expansion.
The standards that have been used as laboratory standards during the δD measurements in this work are listed in Table B.1 in the Appendix and the results of the normalisation are found in Section 5.4.4.

4.2 Seasonal cycles

Snow that has been deposited at high elevation areas of the Greenland ice sheet during present and glacial times has condensated from moisture which mainly originates from the subtropical part of the North Atlantic Ocean [Johnsen et al., 1989]. Temperature dependent isotopic fractionation, caused by different vapour pressure of the $H_2^{16}O$, $H_2^{18}O$ and $HD^{16}O$ molecules during transport from the source area to the depositional site leads to δ variations in the snow that are in phase with seasonal changes of temperature [Epstein and Sharp, 1959; Benson, 1962; Dansgaard, 1964; Dansgaard et al., 1973]. It is these seasonal cycles in the δ profiles that are of interest for absolute dating of ice cores [Hammer et al., 1978]. Figure 4.2 is a simplified illustration of the fractionation process. The numbers represent the δD values for the moisture and the condensate at a given stage in the condensation process. The same scheme applies for the fractionation of oxygen isotopes. During evaporation of ocean water ($\delta \mathrm{D}_{VSMOW}$ = 0‰) and subsequent precipitation, as the air is cooled down on its way to higher latitudes and/or higher altitudes, there is a preferential fallout of heavy components. In the figure this is seen as an evolution towards lower δD values (from dark to light blue colour), on the way in the condensation column (going from South (S) to North (N)). During

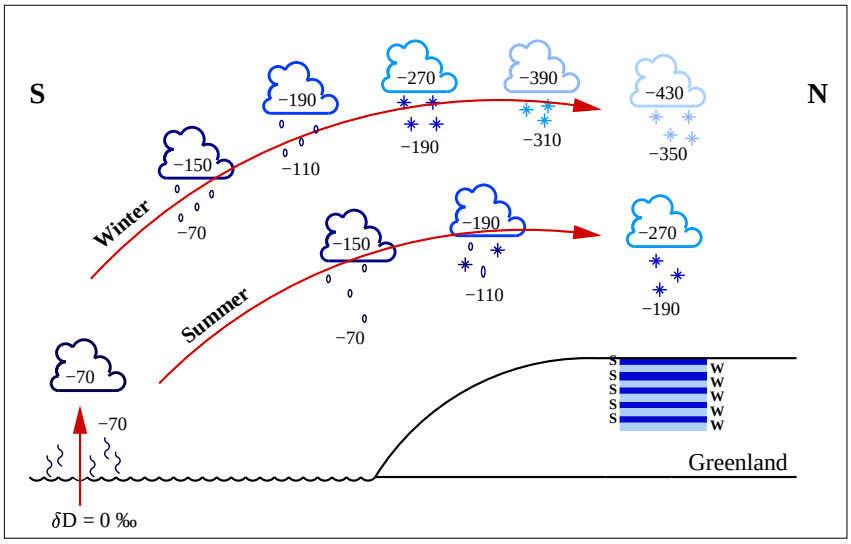

Figure 4.2: Isotopic fractionation of hydrogen isotopes. The H_2O molecules containing ^2H precipitate more easily than the light variants with ^1H. This leads to a depletion of heavy isotopes (low δD values), both in the moisture and in the condensate produced at later stages in the process. In the snow in Greenland the depletion is more pronounced in winter snow (W, light blue) compared to summer snow (S, dark blue).

winter time the airmass is cooled down to lower temperatures than in the summer and the fractionation process extends longer. This gives minimum values of δD during winter (W) times and maximum values during summer (S) times. The seasonal oscillations of δD and δ^{18}O recorded in the ice enables detection of annual layers in the continuous precipitation archive in the Greenland ice cap.

The process that is illustrated in Figure 4.2 can also explain the long-term variations in δ values that is observed to be in phase with changing climatic conditions, as well as the geographical distribution of δ values in cold regions [Dansgaard et al., 1973].

4.3 Diffusion and densification

After deposition the snow is transformed to firn and ice through a densification process. Grain settling and recrystallisation dominate the densification process for depths z above the $z_{close-off}$, which is the depth where the interconnected air channels are transformed to air bubbles ($\rho_{close-off}\sim$830 kg/m^3) [Herron and Langway Jr., 1980]. This is the depth that define the boundary between firn and ice. In the porous firn the H_2O molecules can easily exchange from grain to grain through the vapour phase and hereby cause a (vertical) mixing that results in smoothing of the δ signal, where the high frequencies are gradually obliterated [Langway Jr., 1967; Dansgaard et al., 1973; Johnsen, 1977]. At depths $z > z_{close-off}$ the densification is governed by compression of air bubbles in the ice. When the compression of air bubbles is completed ($\rho\sim$917 kg/m^3), only small changes in the density profile occur, connected to changes in the temperature and pressure conditions. In the ice the δ profiles are influenced by further thinning, due to strain, and by a less strong diffusion effect, caused by self diffusion in ice single crystals [Johnsen et al., 1999, 2000].

The diffusion process can be mathematically described as convolving the initial (unknown) isotope profile $\delta_0(z)$ with a symmetrical Gaussian filter $F(z)$. The measured isotope profile $\delta_m(z)$ is a result of smearing the initial profile with the response function $F(z)$:

$$\delta_m(z) = \delta_0(z) * F(z) = \int_{-\infty}^{+\infty} \delta_0(z) \cdot e^{\frac{(z'-z)^2}{2\sigma^2}}\, dz \tag{4.5}$$

The degree of smoothing is dependant on the diffusion length σ, which is the width of the Gaussian clock in Equation 4.5. The diffusion length describes the mean vertical displacement of a molecule, relative to its initial position, disregarding the movement connected to sinking of the layers. The diffusion length is mainly dependent on the annual accumulation rate, the temperature and the isotopic species.

In the spectral domain the diffusion corresponds to a damping of the initial amplitude A_0 of a harmonic signal in the stable isotope data. This can be written

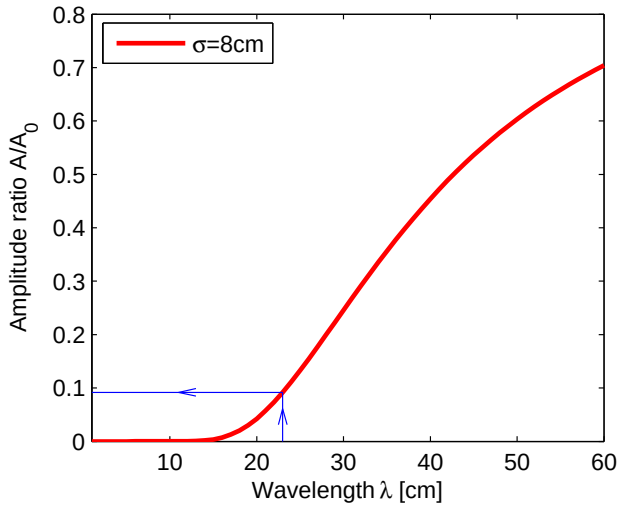

Figure 4.3: Damping of an amplitude of a harmonic cycle in an isotope profi le as a function of λ. For a diffusion length of 8 cm and an accumulation rate of 0.23 m ice per year about 10% of the annual original amplitude is left after diffusion in the fi rn.

as

$$A(k) = A_0(k)\, e^{\frac{-k^2 \cdot \sigma^2}{2}} \tag{4.6}$$

[Johnsen, 1977]. Here A is the amplitude of a signal with wavelength λ and corresponding wavenumber $k = 2\pi/\lambda$ in the measured (diffused) isotope profile $\delta_m(z)$. The exponential factor in Equation 4.6 is the transfer function (frequency response) $\overline{F}(k)$ of $F(z)$.
Similarly, the power spectral densities $P(k)$ of the smoothed profile is related to the $P_0(k)$ of the undiffused profile according to [Johnsen et al., 2000]:

$$P(k) = P_0(k)\, e^{-k^2 \cdot \sigma^2} \tag{4.7}$$

Figure 4.3 shows the damping of the amplitude, represented by the ratio A/A_0, as a function of the wavelength λ. The diffusion length is set to 8 cm, which

corresponds to the typical firn diffusion length in present day Greenland [Johnsen, 1977]. The blue arrow illustrates the expected amplitude ratio in a measured stable isotope profile at a site where the accumulation rate is ∼0.23 m ice per year, which is the case for the GRIP site at present [Johnsen et al., 2000]. For dating purposes, a λ of 20 cm (R ∼0.05) is considered to be at the lower limit for sites in Greenland [Johnsen, 1977].

4.4 Correction for diffusion

From Equation 4.5 and the convolution theorem we have that

$$\overline{\delta}_m(k) = \overline{\delta_0(z) * F(z)} = \overline{\delta}_0(k) \cdot \overline{F}(k) \tag{4.8}$$

where the bars denote Fourier transforms of the corresponding time domain functions. In other words, the Fourier transform of the convolution equals the product of the two individual Fourier transforms $\overline{\delta}_0(k)$ and $\overline{F}(k)$. Rearranging this equation with respect to the unknown initial isotope profile leads to:

$$\overline{\delta}_0(k) = \frac{\overline{\delta}_m(k)}{\overline{F}(k)} \tag{4.9}$$

and

$$\delta_0(z) = \overline{\overline{\delta}}_0(k) = \overline{\left(\frac{\overline{\delta}_m(k)}{\overline{F}(k)}\right)} \tag{4.10}$$

Hence, making an inverse Fourier transform of the right-hand side in Equation 4.9 the initial isotope profile can be reconstructed. This corresponds to a deconvolution or a correction for the smoothing of the initial data. The construction of a spectral filter relies on an estimated diffusion length σ and also the maximum frequency f_{max} in the data to be allowed in the diffusion correction. The diffusion length and the maximum frequency have been estimated by using the Maximal Entropy Method, which will be described in the following sections.

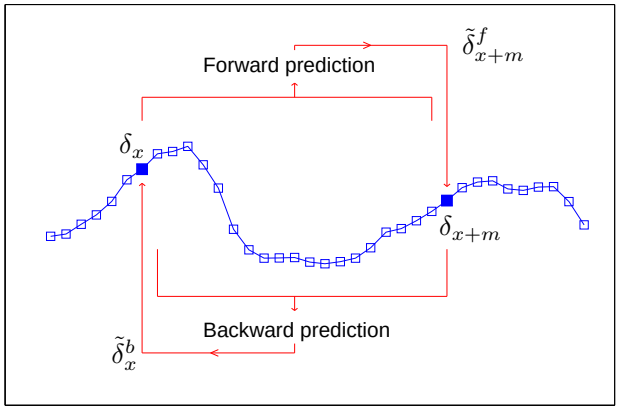

Figure 4.4: MEM prediction in forward and backward direction.

4.4.1 Maximal Entropy Method (MEM)

The Maximal Entropy Method (MEM) has been used for two purposes:
1. For extension of the data sequences in each end, allowing the spectral filter to correct all data points in the sequence, including the endpoints. 2. For calculating the power spectra of the stable isotope series. The power density plots have been used to estimate the diffusion length σ and the cut-off frequency f_{max}.

The MEM method is a form of autoregressive modelling, which in the following will be formulated as a linear prediction problem (see Figure 4.4.). Having a data sequence $\delta_1, \delta_2, \cdots, \delta_N$, of which the mean value is zero, the value δ_{x+m} ($0 < x+m \leq N$) can be predicted as a linearly weighted sum of the m previous samples (forward prediction). The predicted value of sample $x+m$ is denoted $\tilde{\delta}^f_{x+m}$:

$$\tilde{\delta}^f_{x+m} = \sum_{k=1}^{m} a_{mk}\delta_{x+m-k} \tag{4.11}$$

where the subscript m and k in the weight a_{mk} denote the mth-order model and kth coefficient, respectively. Similarly, the value of sample x can be predicted by applying the same prediction filter in the reverse direction. The value $\tilde{\delta}^b_x$ is then

the linearly weighted sum of the m future samples (backward prediction).

$$\tilde{\delta}_x^b = \sum_{k=1}^{m} a_{mk}\delta_{x+k} \tag{4.12}$$

The difference between the actual value of a sample and the predicted value is called the prediction error. The forward prediction error $e^f_{(x+m)m}$ and the backward prediction error e^b_{xm} can be written as:

$$e^f_{(x+m)m} = \delta_{x+m} - \tilde{\delta}^f_{x+m} = \delta_{x+m} - \sum_{k=1}^{m} a_{mk}\delta_{x+m-k} \tag{4.13}$$

$$e^b_{xm} = \delta_x - \tilde{\delta}^b_x = \delta_x - \sum_{k=1}^{m} a_{mk}\delta_{x+k} \tag{4.14}$$

The mean of the squared forward and backward prediction errors of the entire data sequence is then

$$E = \frac{1}{2}\frac{1}{(N-m)} \sum_{x=1}^{N-m} [(e^b_{xm})^2 + (e^f_{(x+m)m})^2]$$

$$= \frac{1}{2}\frac{1}{(N-m)} \sum_{x=1}^{N-m} [(\delta_x - \sum_{k=1}^{m} a_{mk}\delta_{x+k})^2 + (\delta_{x+m} - \sum_{k=1}^{m} a_{mk}\delta_{x+m-k})^2] \tag{4.15}$$

The basic idea of the method is to minimise the prediction power E in Equation 4.15 and hereby to find the best estimations of the coefficients a_{m1}, a_{m2}, $\cdots$, a_{mm}. This is achieved by setting:

$$\frac{\partial E}{\partial a_{mm}} = 0 \tag{4.16}$$

The calculations are performed iteratively by stepwise increasing the autoregressive order from m to m+1. Recursive relationships exist between the filter coefficients, which allow the mth order coefficients to be calculated from the (m-1)th order coefficients that were estimated in the previous pass through the algorithm. The initial condition (m=0) involves no prediction, which reduces Equation 4.15 to

$$E_0 = \frac{1}{N}\sum_{x=1}^{N} \delta_x^2 \tag{4.17}$$

which is simply the power P_0 of the data sequence. The applied algorithm for these calculations can be found in Andersen [1974], who writes the output power P_m of the m+1 long prediction filter as

$$P_m = P_{m-1}(1 - a_{mm}^2) \tag{4.18}$$

and the MEM power spectrum $P(k)$ of the data sequence as

$$P(f) = \frac{P_m \Delta x}{\left| 1 - \sum_{n=1}^{m} a_{mn} e^{2\pi i f n \Delta x} \right|^2} \tag{4.19}$$

where Δx is the data spacing and i is the complex number $\sqrt{-1}$. The frequency f is limited by the Nyquist critical frequency $f_c = 1/(2\Delta x)$, so that $-f_c \leq f \leq f_c$.

Having the estimates of the parameters a_{m1}, a_{m2}, $\cdots$, a_{mm} the prediction filters from Equation 4.11 and 4.12 have been used for extending the data sequences with $p/2$ points in each end, where p in this case is the filter length of the spectral filter.

4.4.2 Estimation of σ

The diffusion length σ can be determined as a function of time and depth by solving the equation

$$\frac{d\sigma^2}{dt} - 2\dot{\epsilon}_z(t) \cdot \sigma^2 = 2\Omega(t) \tag{4.20}$$

Here t is age, $\dot{\epsilon}_z(t)$ is vertical strain rate and $\Omega(t)$ is the diffusivity of the given isotopic species. However, the diffusion length can also be estimated from Equation 4.6 and 4.7, by using estimates of the amplitudes of the annual cycle and the spectral densities for the data series, respectively [Johnsen et al., 2000]. It is the latter method that has been used in this project. The basic assumption is that the original spectral density $P_0(k)$ is white (constant) for high wave numbers. This assumption seems to hold because of strong depositional noise [Fisher et al.,

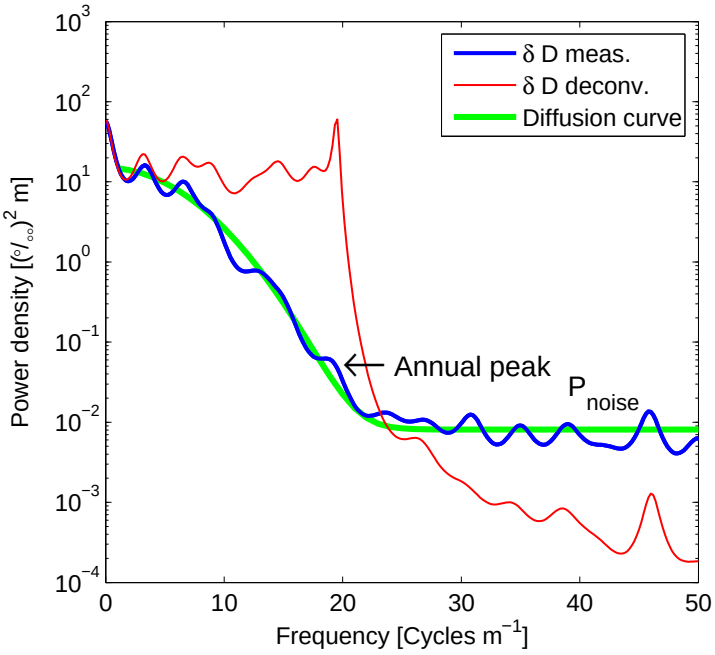

Figure 4.5: A diffusion curve (green) with σ=0.021m reproduces the MEM spectral densities (m=30) of the measured profile (blue). The diffusion in the firn and ice has dampened the amplitudes of the harmonic cycles and at higher frequencies the power densities drop down to the level of measuring error (flat part). The red curve is the power densities of the back-diffused profile (f_{max}=20m^{-1}).

1985]. The diffusion length σ can be estimated by finding the transfer function $\overline{F}(k)$ that corresponds to the observed "colouring" of the spectral density $P(k)$ of the measured profile, as illustrated in Figure 4.5. Similarly, the spectral densities of the reconstructed profile should be flat to accommodate the assumption of white noise in the original data profile.

The green line in Figure 4.5 represents the squared transfer function that can reproduce the observed damping of the amplitudes in the measured isotope data. To account for the observed noise level ε in the measured data, an extra term $\Delta x \cdot \varepsilon^2$ has been added to Equation 4.7.

This method gives a constant σ for the chosen data interval. This is of course an approximation as σ do vary with depth as indicated by Equation 4.20. However, this approximation is considered to be good for each of the stable isotope sections in this work, as the two main factors to influence σ at this depth, strain thinning and changes in climate, do not vary significantly within each data interval.

4.4.3 Choice of cut-off frequency f_{max}

The spectral filter is constructed in such a way that the high frequencies have the strongest amplifications, to counteract the strong damping of the high frequency oscillations. To avoid blowing up noise without any physical meaning, an upper limit has to be put on the frequency for the back-diffusion process. The noise level can be seen, as the nearly flat level at high wave numbers in the spectral densities for the measured isotope profile. Basically, there are two constraints when determining the maximum frequency. Frequencies at the noise level should be excluded from the reconstruction and the annual oscillation should be included, as this is the oscillation that is of interest for dating purposes. However, the choice of maximum frequency f_{max} is not always unambiguous, especially when the annual peak is close to the noise level (as is seen in the example in Figure 4.5). Therefore, great care has to be taken when choosing the maximum frequency. For the isotope sections in this project the cut-off frequency has been chosen manually, as a best compromise between excluding the noise at higher frequencies and including the annual peak.
The results of the diffusion correction are presented in Section 6.2.1.

5 High resolution δD measurements

This chapter includes a theoretical introduction to the method of hydrogen isotope analysis of water samples and a description of the experimental method used for high resolution δD measurements on the ice samples from the GRIP core. Furthermore, some problems encountered during data acquisition and methods to handle these problems are presented. The last part of the chapter is devoted to the first step of data processing of the hydrogen isotope data, from the raw data to normalised data.

5.1 Introduction to Stable Isotope Ratio Mass Spectrometry (SIRMS)

The method of using a magnetic-sector mass spectrometer for determination of isotope ratios of for example C, O, S and H in gases has become widespread since it first was presented by Nier [1947]. The basic concept of such a mass spectrometer is to make an ion beam of the gas and to separate and collect ions of different masses by leading the ions through a magnetic field, which deflects the ions into different paths according to their masses. There are numerous books and articles on this method, see for example Platzner et al. [1997]. The gas molecules are ionised in the ion source of the mass spectrometer by an electron bombardment. Some of the gas molecules will collide with the electrons and these molecules are then transformed into ions, mostly singly-charged positive ions. For the case of hydrogen gas the primary ions are H_2^+ and HD^+, with mass 2 and 3, respectively.

The ions are accelerated by a potential V and formed into a well-defined beam and lead through a source slit. The ions are injected into a uniform magnetic field B and the magnetic force separates the ions into beams of different radii corresponding to their different masses. The trajectory of an ion with mass m and charge z is described by the classical equation:

$$\frac{m}{z} = \frac{B^2 r^2}{2V} \tag{5.1}$$

where r is the radius of the circular path. Each beam enter a collector through a narrow slit, which is positioned in accordance with the trajectory described by Equation 5.1. A multiple Faraday collector system allows simultaneous collection of all relevant beams. The ion current i from the cup, which is found by integrating the peak in the chromatogram (see Appendix C), is proportional to the number of incident ions of the particular radius and hence the partial pressure of the corresponding isotopic molecular species in the gas. However, for stable hydrogen isotope analysis the current $i(3)$, measured at the the mass 3 collector, is influenced by the production of H_3^+ ions in the ion source:

$$H_2^+ + H_2 \longrightarrow H_3^+ + H \tag{5.2}$$

The H_3^+-production is proportional to the square of the partial pressure of the hydrogen in the ion source [see Platzner et al., 1997, p. 26], hence the current ratio $i(3)/i(2)$ can be written as

$$\frac{i(3)}{i(2)} = \frac{HD^+ + H_3^+}{H_2^+} = \frac{HD^+}{H_2^+} + \frac{k \cdot [H_2^+]^2}{H_2^+} \tag{5.3}$$

or

$$\frac{HD^+}{H_2^+} = \frac{i(3)}{i(2)} + k \cdot i(2) \tag{5.4}$$

The H_3^+-correction constant k is dependent in the residence time of H_2^+ ions in the ionisation volume and can be directly measured. As mentioned in Section 4.1 the isotopic composition of a sample is reported as a relative deviation from a standard (δ notation). This is done to work around any possible biases of the system, for

example in the collectors. Therefore, a sample and a working standard (reference gas) are introduced alternately into the ion source under identical conditions.

There is a vast diversity of sample preparation systems to connect to an SIRMS. The purpose of the inlet system is to convert the natural occurring sample into an elementary gas, while preserving the fingerprint of the isotopic composition of the original sample. For δD or δ^{18}O analysis of water samples there are two main methods of converting the liquid sample to a gaseous phase: Reduction over a hot metal or equilibration with CO_2 or H_2 gas. The hydrogen isotope analysis of the melted ice samples from the GRIP ice core was performed by using a chromium reduction technique. Section 5.2.1 gives a description of the mass spectrometer and the inlet system that were used for the detailed δD measurements in this project.

5.2 δD measurements on GRIP ice core samples

The δD measurements were performed at the AMS ^{14}C Dating Centre, Department of Physics and Astronomy, University of Århus in Denmark during several periods from August 2002 to November 2003 (see Table D.1 in the Appendix).
The SIRMS at the AMC ^{14}C Dating Centre in Århus was new when these measurements started in August 2002, which meant that routines with sample preparation and data acquisition, as well as the operational settings of the inlet system and the mass spectrometer itself, were adopted continuously according to the growing experience. Some major problems with amongst others the auto sampler and the ion source of the mass spectrometer caused the measurements to be delayed and spread out in time.

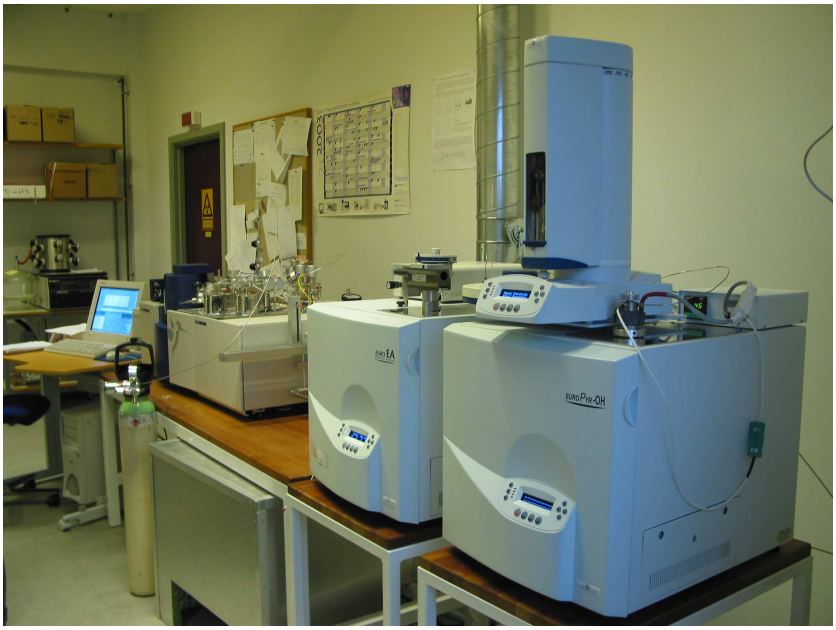

Figure 5.1: Experimental set-up. From right to left: Liquid auto sampler, elemental analyser, Isoprime mass spectrometer and computer. See Figure 5.2 for a schematic illustration.

5.2.1 Experimental set-up

The δD measurements were performed on a Micromass[1] IsoPrime Isotope Ratio Mass Spectrometer (IRMS) [Morrison et al., 2001; Micromass]. The IRMS is integrated with an elemental analyser (EuroPyrOH-3100) and a combined auto injector and liquid auto sampler (LAS EuroAS300), both manufactured by Eurovector. The setup is dedicated to continuous flow (CF) hydrogen pyrolysis where the sample gas is carried like a small bubble in a continuous and constant flow of helium (He) through the elemental analyser into the ion source of the mass spectrometer. The IRMS system is controlled from a computer using MassLynx software [Micromass]. See Figure 5.1 and 5.2.

[1]Now GV Instruments

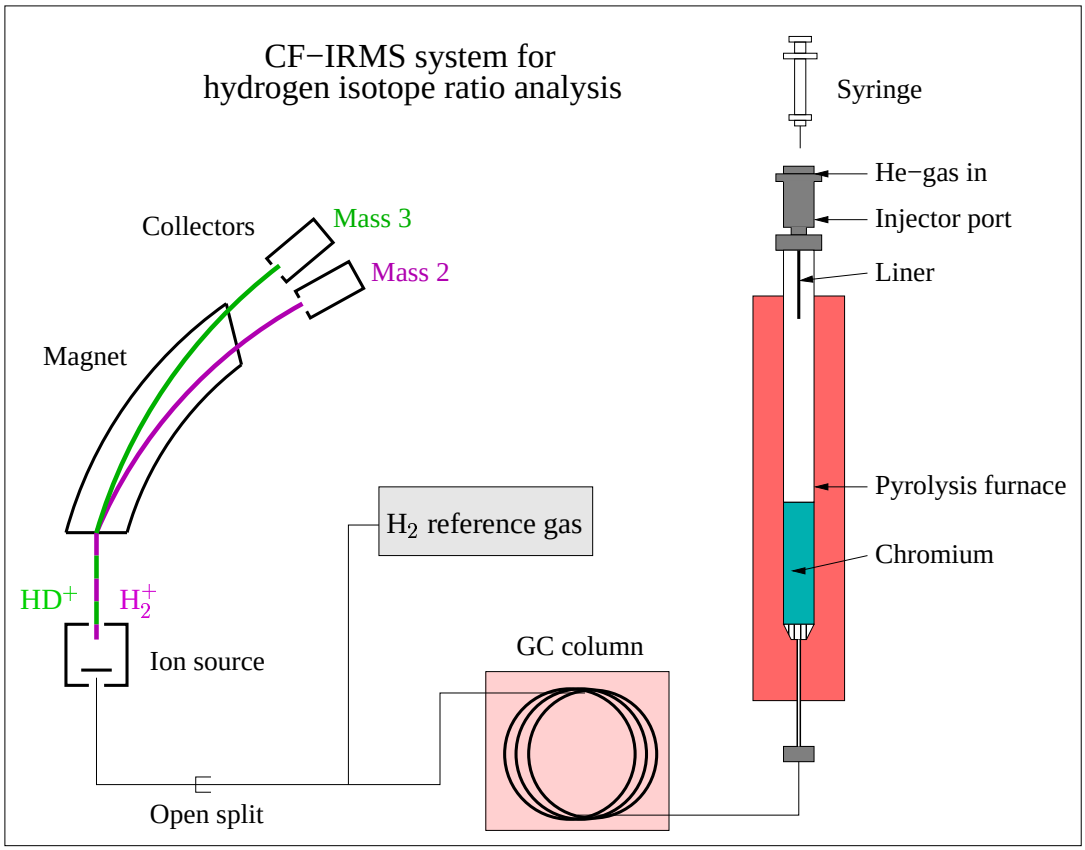

Figure 5.2: Schematic illustration of the continuous flow isotope ratio mass spectrometer (CF-IRMS) system used for the δD measurements.

The liquid auto sampler provides a sample capacity of up to 110 and the liquid samples are kept in septa-sealed vials (2 ml capacity), which are placed onto the carousel of the auto sampler. An auto injector with a syringe automatically injects a certain amount (0.3-0.5 μlitre) of sample from the vial into the heated septa-sealed injection port ($\sim$160 °C), where the sample is immediately transformed to water vapour. Prior to injection the needle is washed a number of times (1-3) with 1 μlitre of the sample water to minimise the contamination from the previous sample. The sample sequence, the injection parameters (such as sample volume, number of wash cycles, injection time etc.) is set by the aid of a data system in

the liquid auto sampler.
After injection the sample follows the He flow through a stainless steel probe, called an injection port liner, down to pyrolysis unit in the elemental analyser. The pyrolitic reactor is held at $\sim$1050 °C and it consists of a quartz tube packed with chromium powder, silica chips and quartz wool at the lower end (see Figure E.2 in Appendix E). Due to the high temperatures in the furnace the water vapour is reduced to hydrogen gas by the chromium:

$$2\mathrm{Cr}\,(s) \;+\; 3\mathrm{H_2O}\,(g) \;\longrightarrow\; \mathrm{Cr_2O_3}\,(s) \;+\; 3\mathrm{H_2}\,(g) \tag{5.5}$$

The formed H_2-gas is led through a gas chromatographic column (GC packed column 1.5 m, Eurovector), where the speed of the flow is reduced to ensure that the peak shape is adequate for the integration software, and possible pollutant species are time separated from the gas subjected to analysis.
A small portion of the sample is drawn by the vacuum ($\sim 10^{-6} - 10^{-9}$ Torr) within the mass spectrometer through an open split and subsequent isotopic analysis follows as described in Section 5.1. A pulse of reference H_2 gas is led into the mass spectrometer through the same open split as the sample gas and isotopic analysis of the reference gas allows calculation of δD relative to the reference gas. The mass 3 collector is fitted with an electrostatic energy filter to remove the signal from the tail of the helium peak [Merren, 2000; Morrison et al., 2001].

5.2.2 Sample preparation

Cutting of ice samples

The ice samples for high resolution δD measurements have been cut from three depth intervals in the GRIP deep ice core that was drilled during the years 1989-1992 [GRIP Members, 1993]. The three intervals, which are called δD Interval I, δD Interval II and δD Interval III are found close to $\sim$1700 m. This corresponds to the climatic period Bølling-Allerød, $\sim$14-15 ka BP. See Table 5.1 for detailed description of the depth and length (L) of the intervals, as well as the number

Interval	*Depth*	*Bags*	*Period*	*L*	*No.*
	m			m	
δD I	1714.35 - 1719.85	3118 - 3127	OD	5.50	550
δD II	1729.20 - 1735.25	3145 - 3155	Mid B	6.05	605
δD III	1744.6 - 1755.05	3173 - 3191	End Ost D + Start B	10.45	1045
Total				22.00	2200

Table 5.1: Ice sampling from the GRIP deep core. The column $Period$ indicates which climatic periods the intervals belong to. OD, B, and Ost D denote the periods Older Dryas, Bølling and Oldest Dryas, respectively.

($No.$) of samples in each interval and the bag[2] numbers. The ice has been stored at -26 °C and the sampling where performed in the -15 °C cold freezer at the Niels Bohr Institute at the University of Copenhagen in Denmark in June-August 2002.

A total of 2200 ice samples were cut on a band saw. The core used for sampling was mainly leftover of the so-called DK-bag, apart from a few bags where the main core was used. Each bag was cut horizontally into a thin rod. Loose ice particles where cleaned off by scraping with a knife and swiping with a soft brush. The rod was then carefully divided into 55 samples along the core. A small pencil mark for every centimetre was used as a guideline when cutting the 1 cm pieces. Each sample constituted a total volume of $\sim$2 cm^3. The samples were given names according to the bag number and the division of into 55 samples per bag, so that the first (top) sample in bag 3174 is named 3174-1 and the last (bottom) sample is called 3174-55. The ice samples were put in numbered Coulter beakers of 50 ml with snap-cap. As these bottles are not completely air-tight, the samples were melted at room temperature and immediately poured into numbered 10 ml plastic bottles with screw-cap, which were kept frozen at -15 °C until measurements were performed.

[2]For practical reasons the ice core is stored in 55 cm long pieces. Such a piece is called a bag. Bag number 1 is the top bag of the total ice core starting at surface and the numbers increase with depth.

Preparation of melted ice samples

Prior to δD analysis on the SIRMS (as described in Section 5.2.1), the samples were melted at room temperature and 1 ml of each sample was poured into numbered 2 ml septa-sealed glass vials by using a pipette. The vials were then placed onto the auto sampler for δD analysis. For every new water sample a new dry tip was adhered to the pipette. The vials, the septa and the tips for the pipette were all used several times to minimise the costs. To ensure that no contamination occurred by reusing these items, all the material was dried for at least 24 hours at 80 °C prior to preparation of a new set of samples. During the whole process of sample preparation, from cutting the ice samples to the point of measurements, attention was paid to avoid evaporation and isotopic fractionation, as well as contamination from other samples or external sources.

5.3 Instrumental effects

5.3.1 Drift

When performing δD analysis of hundreds of samples during one run, a minor trend is often seen in the data. If the same sample is measured at different times during the run, the δD values in the beginning and at the end of the run may differ significantly, up to several ‰ [Werner and Brand, 2001; Nelson and Dettman, 2001; Brooks et al., 2004] .When the isotopic ratios of the reference gas R_{Ref} are changing during the run, this will introduce an artificial trend in the δD values of the samples. This drift can be checked and corrected for by measuring a standard sequence at both ends of the run and by investigating the trend of δD value of this standard.

In this project the drift correction has been performed under the assumption that the drift is linear in time. A drift correction constant a has been acquired for each run, by making a linear regression where the δD values of a standard, which is

measured repetitively in the beginning and in the end, are used as input. The slope a of the fit is a measure of the drift and for runs where drift is observed, a has been used to correct all measured δD values in the run according to:

$$\delta \mathrm{D}_{x/Ref}^{Drift} = \delta \mathrm{D}_{x/Ref}^{Raw} - a \cdot x \tag{5.6}$$

where x is the sample number in the run and $\delta \mathrm{D}_{x/Ref}^{Raw}$ and $\delta \mathrm{D}_{x/Ref}^{Drift}$ are the measured and the drift corrected δD values of sample x, respectively, relative to the reference gas. Only injections where the δD values were undisturbed of memory effect (will be described in Section 5.3.2) were used in the linear regression. Results from the control of and correction for drift are found in section 5.4.2.

To simplify the notation, the subscript "Ref" will be omitted in cases where it is clear that the δ value is relative to the reference gas. This means that $\delta \mathrm{D}_{x/Ref}^{Raw}$ will be written as $\delta \mathrm{D}_{x}^{Raw}$ in the following sections. The subscript "Ref" will be introduced again when we speak about normalisation to the VSMOW-SLAP scale.

5.3.2 Memory effect

CF-IRMS-systems are known to suffer from a so-called memory effect which is a term used to describe the contamination of the analysed water sample with reminiscences of previous samples. The memory effect has been described by several authors, e.g. [Morse et al., 1993; Vaughn et al., 1998; Donelly et al., 2001; Morrison et al., 2001; Nelson and Dettman, 2001] and it is believed that the memory effect is mainly caused by water adhering to inner surfaces of the inlet system. When measuring samples of different isotopic composition, the memory effect leads to displaced δD values and have a negative influence on the accuracy. Ignoring any drift of the system, the true value[3] $\delta \mathrm{D}_{x}^{True}$ of a sample x is

$$\delta \mathrm{D}_{x}^{True} = \delta \mathrm{D}_{x}^{Raw} + F_x \tag{5.7}$$

[3]Relative to the reference gas

where δD_x^{Raw} is the measured value and F_x is the offset in ‰ for the sample x. In this project the drift correction has been made prior to the memory correction, therefore the δD_x^{Drift} has been used instead of δD_x^{Raw}. The offset term is dependent on the difference (Δ_x) in δD value between the sample x and the previous one. Furthermore, the offset term varies from machine to machine, as well as it is dependent on the operational settings at the time of measurement [Morse et al., 1993], so a thorough investigation and routinely control of the memory effect is recommended. One way to deal with the memory effect is to measure each sample several times repetitively, until the memory effect is negligible, and only use the last repetition(s) as true value(s). Another approach is to develop and apply a correction algorithm that corrects for the memory effect. The latter method has been used in this project, partly to reduce the time and costs spent on laboratory work and partly because the consecutive and high-resolution ice core samples in this study seldom differ more than 15 ‰ from one sample to the next; and normally only around 5 ‰. The low inter-sample transition steps means that the offset F_x becomes relatively low for a given memory effect. As will be outlined in Section 5.4.3, the low inter sample transition steps make the correction algorithm superfluous, provided that the memory effect is sufficiently low. However, a memory correction has been successfully applied within periods of higher memory effect. The methods that have been used in this project to investigate, model and correct for the memory effect will be outlined in the following subsections.

Fractional memory effect

The fractional memory effect ϕ_x from a sample x-1 to the next sample x can be described as

$$\phi_x = \frac{\delta D_x^{True} - \delta D_x^{Meas}}{\Delta_x} \tag{5.8}$$

where Δ_x is the true difference in δD (transition step) between the samples x-1 and x. By definition the memory effect is positive and it is normally given in

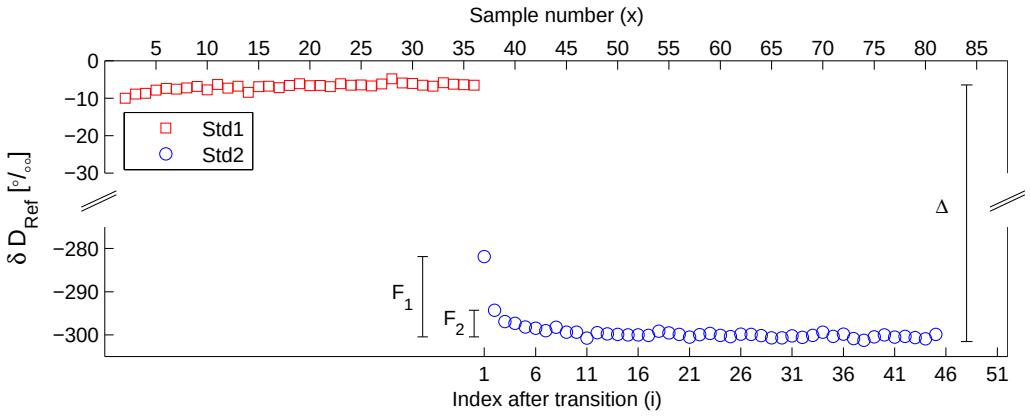

Figure 5.3: Standard sequence

percent. By combining equation 5.7 and 5.8 we get

$$\phi_x = \frac{F_x}{\Delta_x} \quad or \quad F_x = \phi_x \cdot \Delta_x \tag{5.9}$$

Hence, to get information on the offset F_x for a sample x we need to know the fractional memory effect for the actual settings of the system and also the transition step Δ_x. For this purpose, it is useful to measure standards of different isotopic composition alternately, as described in the following.

Standard sequences

In this study, standard sequences were set up, where at least two standards, with a transition step $\Delta > 100‰$, were measured consecutively with n repetitions of each standard ($n > 18$). The standard sequences were placed in the beginning and/or at the end of certain runs (as seen in Table D.1). Figure 5.3 shows an example of such a standard sequence. It can be seen that the first standard (Std1) not only affect the first repetition of the second standard (Std2), but several of the following injections of Std2, until the memory effect approaches zero. The offset terms F_1 and F_2 for the first and second injection of Std2, respectively, are

shown in the figure. The long term trend of the memory effect demands that a fractional memory coefficient is determined for each of the repetitions of Std2 that is influenced by the memory effect. For a standard sequence the fractional memory coefficient can be found by a modification of Equation 5.8, where the transition step Δ is the isotopic difference between the two standards:

$$\phi_i = \frac{\left\langle \delta \mathrm{D}_{Std2}^{True} \right\rangle - \delta \mathrm{D}_i^{Meas}}{\left\langle \delta \mathrm{D}_{Std2}^{True} \right\rangle - \left\langle \delta \mathrm{D}_{Std1}^{True} \right\rangle} = \frac{F_i}{\Delta} \tag{5.10}$$

where $\left\langle \delta \mathrm{D}_{Std2}^{True} \right\rangle$ and $\left\langle \delta \mathrm{D}_{Std1}^{True} \right\rangle$ are true values[4] of Std1 and Std2, respectively, found by taking an average of the last 5 injections; assuming that the memory effect is absent for these repetitions. The index i denotes the injection number after the transition, i.e. i=1 corresponds to the first injection of Std2, i=2 corresponds to the second injection of Std2 and so on. A fractional memory coefficient is determined for each of the repetitions of Std2.

Modelling the memory effect

Analytically the memory effect has been found to be well described by a sum of two exponential decay functions. For each standard sequence, the fractional memory coefficients ϕ_i from Equation 5.10 have been used as input to a least squares fit of model $f(i)$:

$$f(i) = c_1 \cdot e^{k_1 \cdot i} + c_2 \cdot e^{k_2 \cdot i} \tag{5.11}$$

The constants c_1, c_2, k_1 and k_2 are determined by the least squares' fit and they reflect the magnitude (c_1 and c_2) and the range (k_1 and k_2) of the memory effect. An example of an analytical fit is seen in the left panel of Figure 5.4.

For all the measured standard sequences the fractional memory coefficients and the model parameters have been calculated and determined. The models have been used for correction of unknown samples and have also served as an analytical tool for judging which operational setting that gives the least memory effect

[4]Relative to the reference gas

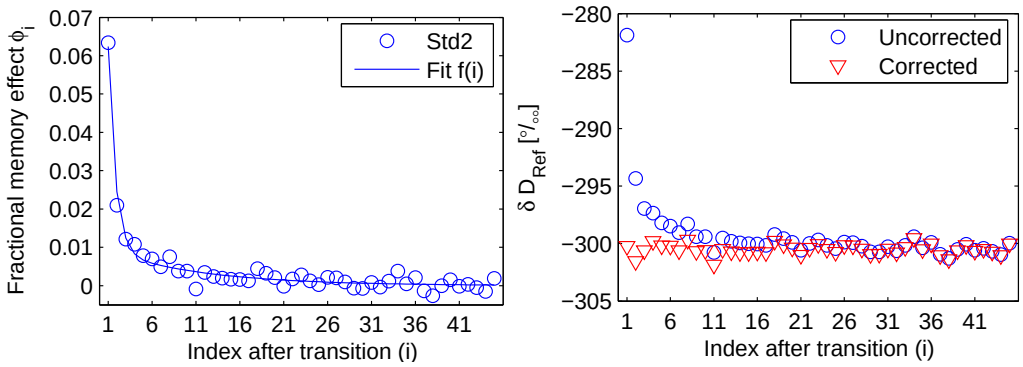

Figure 5.4: Model of memory effect.

within δD analysis on a CF-IRMS [Olsen et al., In prep.].

Correction for memory effect

The fractional memory coefficients that have been derived from the standard sequence have been used to correct measured samples in a run, by using Equation 5.7 and Equation 5.12, where the latter is a rewritten form of Equation 5.9 that takes into account that the memory affects not only the next sample, but several of the following injections. The offset term F_x is a sum of the offset terms stemming from the z previous samples that have influenced the δD_x^{Raw}:

$$F_x = f(1) \cdot \Delta_x + f(2) \cdot \Delta_{x-1} + \cdots + f(z) \cdot \Delta_{x-z+1} \tag{5.12}$$

The subscript x indicates the index of the sample to be corrected and z is the number of previous samples that affect the δD value of sample x (i.e. filter length). The transition step Δ_x is the difference between the value of sample x and $x-1$, Δ_{x-z+1} between sample $x-z+1$ and $x-z$ and so forth. The coefficients $f(i)$ are the fractional memory coefficients which were determined by the model in Equation 5.11. $f(1)$ is the fractional memory coefficient stemming from the preceding sample $x-1$ and $f(2)$ from the second last sample etc.. Of the total

memory effect for sample x the last sample $x-1$ will have the greatest contribution and the memory effect then falls off towards zero for sample $x - z + 1$, i.e.:

$$f(1) > f(2) > \cdots > f(z) \tag{5.13}$$

The first z samples of a run can not be corrected as the pre-start history of the system is unknown. This problem can be overcome by measuring several repetitions of a standard in the beginning. The correction was first calculated from the measured inter sample transition step. Then the correction was refined iteratively by using the new transition step, calculated from the corrected data. The iteration was performed until the calculated transition step remained unchanged from one iteration to the next.

5.4 Data processing

This section consists of a description of the first part of the data processing of the δD data, from raw values to normalised values.

5.4.1 Raw

As described in Section 5.1, the H_3^+-corrected ion currents have been transformed to isotopic ratios R_x and R_{Ref} of the sample and the reference gas, respectively. The raw δD value of sample x relative to the reference gas has been calculated according to Equation 4.1 which becomes:

$$\delta \mathrm{D}_{x/Ref}^{Raw} = \left(\frac{\left(\frac{[D]}{[H]}\right)_x - \left(\frac{[D]}{[H]}\right)_{Ref}}{\left(\frac{[D]}{[H]}\right)_{Ref}} \right) * 1000 \text{ ‰} \tag{5.14}$$

The drift- and memory free values from the δD measurements normally have standard deviations of 0.3-0.5 ‰.

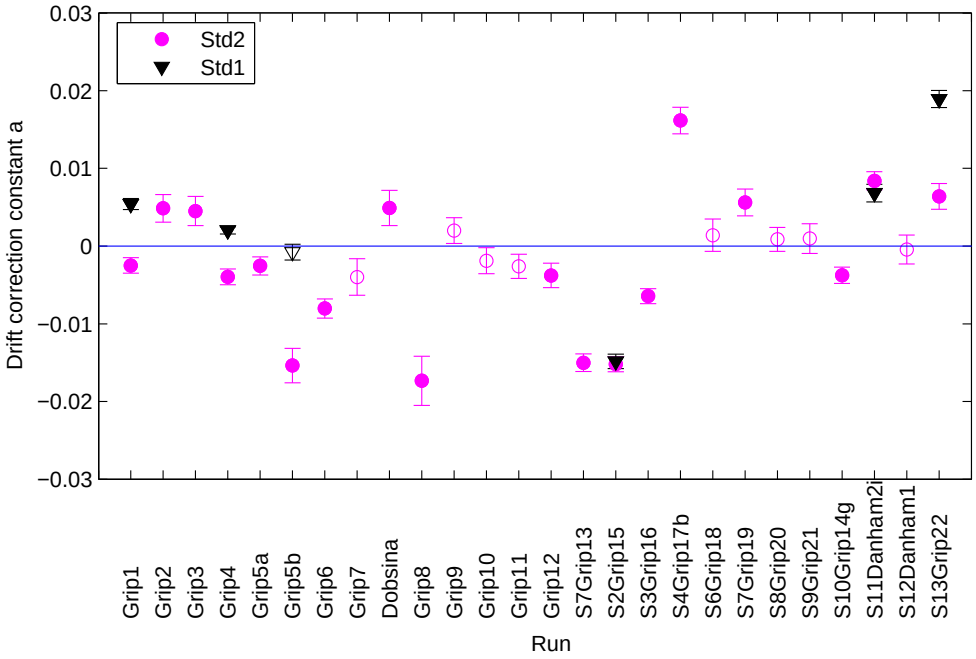

Figure 5.5: Drift correction constants calculated from different runs measured at different times within a period of 15 months. Full circles and full triangles indicate drift correction constants that have been used for correction of samples. Open markers are runs that have not been drift corrected.

5.4.2 Correction for drift

As described in Section 5.3.1 a drift correction constant a has been computed for each run. Figure 5.5 shows the drift correction constant a and the standard deviation from each of the runs where it was possible to calculate the drift (i.e. standards in both ends). The horizontal line marks the level of no drift. The open circles and triangles represent runs that are interpreted to be free of drift, while the full markers symbolise runs with a drift. The latter group includes runs where the $a \pm 1\sigma$ does not enclose the zero-line and, additionally, where the correlation

(R=0.65-0.9) from the regression is significant or highly significant[5]. Both negative and positive trends are found and the magnitude of the slope spans the range from -0.017 to +0.019. A slope of 0.019 corresponds to a change in δD value of $\pm$1.9‰ per 100 injections, which is greater than the standard deviation on the measurements and therefore significant.

Drift correction has been performed on those runs that are indicated with a solid marker in Figure 5.5. All samples in the respective runs have been corrected by applying Equation 5.6.

For some runs it was possible to calculate an a value from both Std1 (triangle) and from Std2 (circle). Surprisingly, it is observed that two different correction constants from the same run do not necessarily show the same magnitude of drift, in some cases, they are even not on the same side of the zero-line (Grip4 and Grip1). For runs where two correction constants were obtained, an average value of a was used for the correction of the measured values. Brooks et al. [2004] similarly report about drift at different rates for standards of different isotopic composition. They hypothesise that variable conditions in the chromium reactor affect the isotope ratio of different water standards in different ways, leading to a differential drift.

No correction constant could be computed for the runs Danham2, S8Grip14 and S4Grip17, as they were aborted before completion of the run. Therefore, no drift correction were performed for these three runs. However, none of the regular ice core samples from these runs have been included in the further analysis, as they were remeasured at a later stage. These runs have only been included in the data analysis because they were used in the normalisation process.

5.4.3 Correction for memory

After having applied the drift correction, the δD_x^{Drift} values have been corrected for inter sample memory.

[5] Significant and highly significant means that there is a 5% and 1% probability, respectively, of getting a correlation coefficient as large as the observed value, when the true correlation is zero.

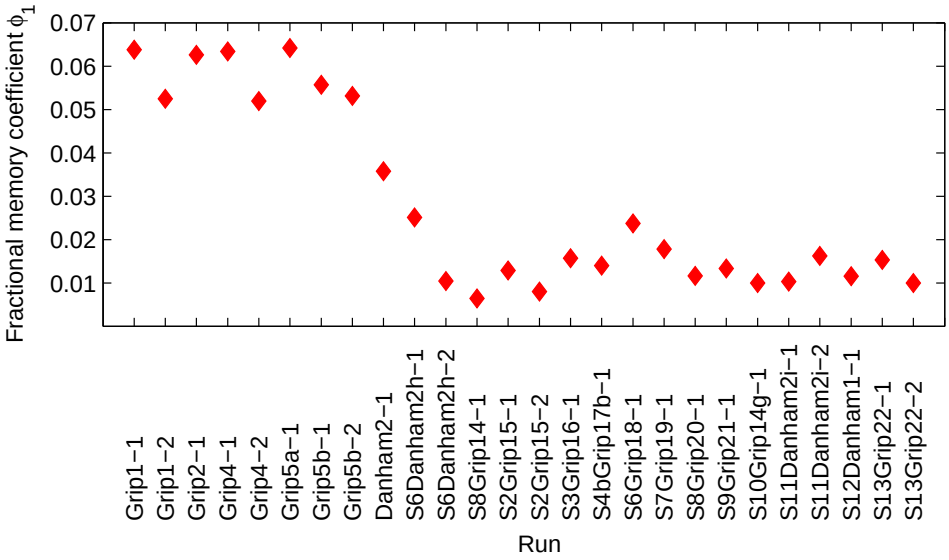

Figure 5.6: Memory. The memory has been calculated from runs with standard sequences. The numbering 1 and 2 at the end of the run names are used to discriminate between different standard sequences in one run.

Fractional memory coefficients ϕ_i were calculated from standard sequences as described in Section 5.3.2. Figure 5.6 displays the magnitude of the memory effect, represented by the first fractional memory coefficient ϕ_1, as observed in the different standard sequences. The most prominent feature in this plot is that the memory effect separates into two different levels. For the first runs (Grip1 to Danham2) the memory effect is 5.6$\pm$0.9 % and for the rest of the runs it is 1.4$\pm$0.5 %. The reduction of memory effect occurred at the same time as the liner in the injection port was changed to another type (see Figure E.1 and Olsen et al. [In prep.]). Morrison et al. [2001] report about memory effects of $\sim$1% on the same CF-IRMS system as the one used in this study. Hence, the memory from the low memory group is acceptable at the expected level.

A 5.6% memory necessitates a memory correction, as a sample difference of 15‰ between the ice core samples will give a offset of $\sim$0.8‰, which is greater than the measuring error. The memory correction was performed as described in Sec-

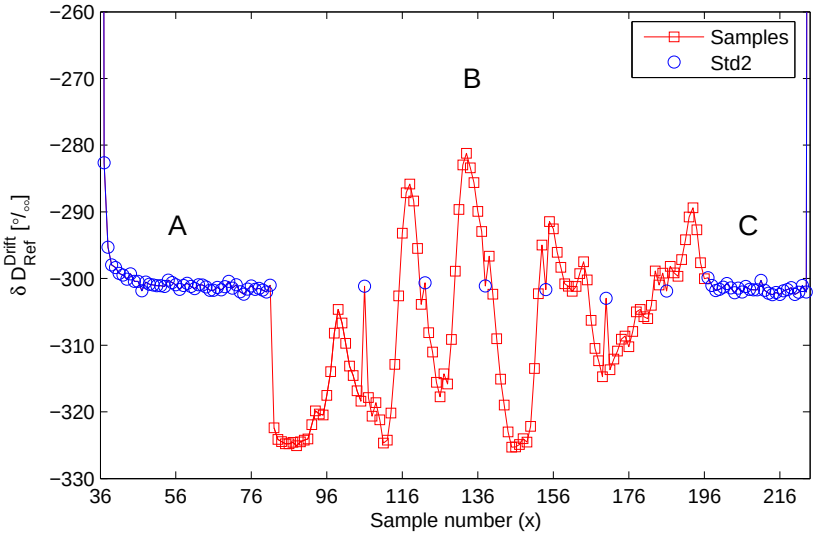

Figure 5.7: A, B and C sequences. The standard Instaar GW1 (Std2) is measured repetitively before (A) and after (C) the regular ice core samples and it is also injected in between (B) the samples. This example is from run Grip4.

tion 5.3.2 for the samples that belong to the period of high memory. For runs with a lower memory of 1.4% it is considered that a memory correction is not required, because the offset for the same inter sample transition step, would be ∼0.2‰, which is well within the measuring error.
For the same reason, most of the standard sequences within the low memory effect group were shorter than those in the in high memory effect group. This meant that the runs were shorter and more time efficient.

Validity of the memory correction

The right panel of Figure 5.4 shows how the memory affected injections of Std2 are successfully corrected down to the “true” level. However, this is not surprising, as the correction model is derived from the very same data set. A way of testing the memory correction model is to treat a standard as a regular sample,

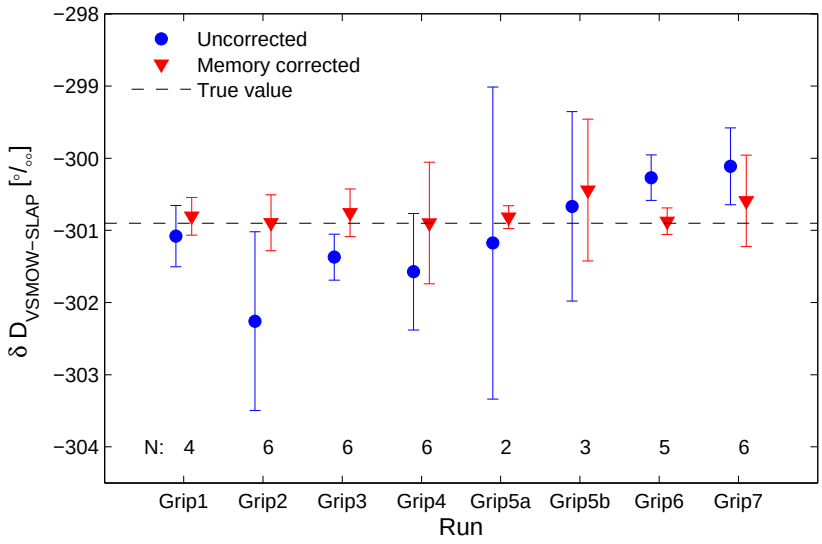

Figure 5.8: Validity of memory correction. Memory corrected and uncorrected mean values of Instaar GW1 from B sequences from several runs. The numbers at the bottom of the fi gure correspond to the number of B-values that are used to calculate the mean values and corresponding standard deviations for each of the runs.

as illustrated in Figure 5.7. The standard Std2 has been measured repetitively in both ends of a run (sequence A and C) and also in between a series of samples (sequence B). A proper correction algorithm should correct the values of the standard in sequence B so that the difference between these values and the true value is within the measuring error only. Also, the scatter in the data should be reduced. Figure 5.8 displays the uncorrected and corrected mean δD values of Std2 (Instaar GW1) from sequence B from several runs. The values are normalised to the VSMOW-SLAP scale so that inter-comparison is possible. It is seen that the corrected values are consistent with the true value, which is satisfactory within the margins of error for all runs, while it is outside 1σ for half of the runs for the uncorrected values. On the basis of this, it must be inferred that the correction algorithm satisfactory correct for the memory effect.

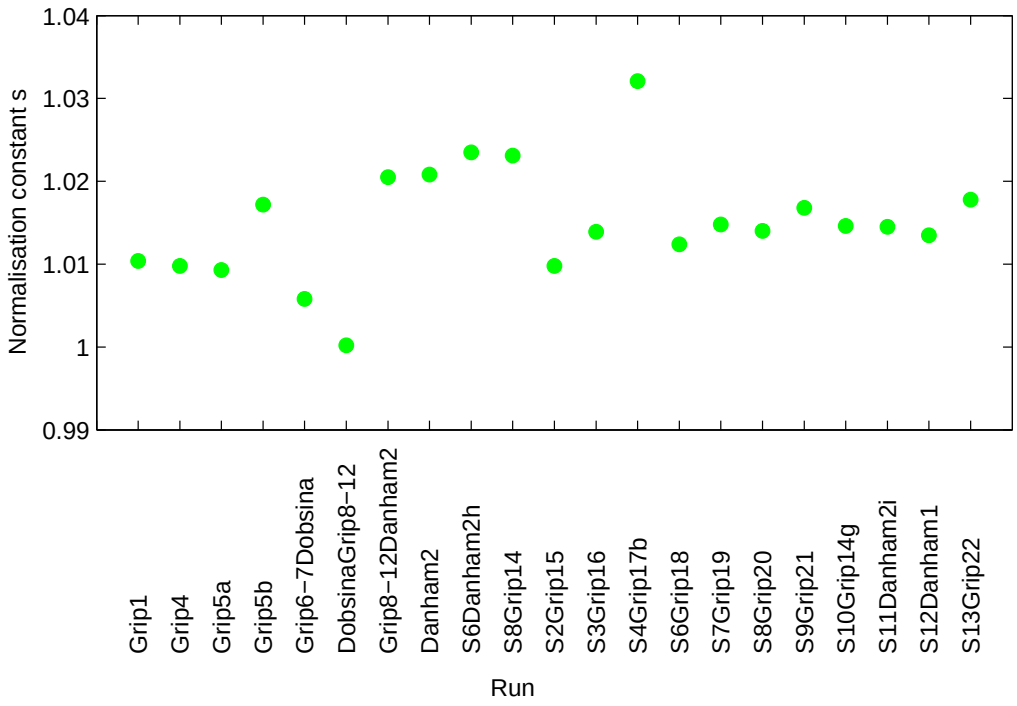

Figure 5.9: Normalisation constants over time.

5.4.4 Normalisation to the VSMOW-SLAP scale

The drift- and memory corrected values have been expressed relative to VSMOW and normalised to the VSMOW-SLAP scale by making a linear regression as described in Section 4.1.1. The normalisation constants can be seen in Figure 5.9. In runs with one standard only, a scaling coefficient has been obtained by using two standards from different runs within the same time period. This is the case for the runs Grip6-12, Dobsina and Danham2h. From Figure 5.9 it is seen that the normalisation constant scatter from a minimum value of 1.000 (DobsinaGrip8-12) to a maximum value of 1.032 (S4Grip17b), where the latter normalisation constant corresponds to a measured SLAP-value of 414.7‰, as opposed to the assigned

value 428‰. According to [Meijer, 2001] "laboratories are likely to have serious problems if they are finding unnormalised δ^2H values for SLAP that deviate from the assigned values than by more than $\sim$10‰". A scale contraction giving a deviation of 10‰ corresponds to a normalisation constant of 1.026. This is indicating bad instrument performance for the run S4Grip17b. All other normalisation constants are less than 1.026, however, there are a few normalisation constants that are close to this value. Inter-laboratory comparison (ring tests) organised by the International Atomic Energy Agency [Meijer, 2001] and by Brand and Coplen [2001] show that unnormalised values of SLAP show a wide range at the different laboratories (from -384‰ to 441‰ in the actual ring tests).

The normalised numbers from the different runs have been concatenated to three δD series corresponding to Interval I, II and III (can be seen in Figure 6.1). These data sequences are now ready to be corrected for diffusion, as will be described in Section 6.2.1.

6 High resolution GRIP data

This chapter presents the high resolution GRIP data that have been used for the annual layer counting of Bølling-Allerød and Younger Dryas periods in the GRIP ice core. The data are listed in Table 6.1. The table displays the depth intervals of the data, the length (L) of each data sequence and the sampling interval Δx. The column $Filter$ indicates if the data has been deconvoluted (Dec) or high-pass filtered (Hpf). The column $Period$ shows which period the data series cover Bølling (B), Older Dryas (OD), Allerød (A) of Younger Dryas (YD) the series cover.

6.1 ECM, dust and ion concentrations

The Electrical Conductivity Measurement (ECM) profile from the GRIP core is presented in Taylor et al. [1993]. The direct-current electrical conductivity measurements was performed by dragging to electrodes with a potential difference of 1250 V along a clean surface of the ice core. The current flowing between the electrodes is a measure of the acidity in the ice. The values were originally gathered continuously for every 1-2 mm of the core, depending on the speed of the electrodes along the core. This profile was then re-sampled to 1 cm resolution. In this project the re-sampled ECM-profile has been used for the annual layer counting within the Bølling-Allerød period. For the annual layer counting of the Younger Dryas section it was possible to include the original profile in 1-2 mm resolution.

Data	*Depth*	*L*	Δx	*Filter*	*Period*
	m	m	m		
δ^{18}O I	1689.61 - 1703.35	13.75	0.01	Dec	Mid A
δ^{18}O II	1749.01 - 1750.10	1.10	0.01	Dec	End Ost D + Start B
δD I	1714.35 - 1719.85	5.50	0.01	Dec	OD
δD II	1729.20 - 1735.25	6.05	0.01	Dec	Mid B
δD III	1744.6 - 1755.05	10.45	0.01	Dec	Start B
NO_3^- ‡	1624.27 - 1753.3	129.03	0.001-0.01		YD + BA
Dust ‡	1624.27 - 1753.3	129.03	0.001-0.01		YD + BA
Ca^{2+} †	1624.27 - 1753.3	129.03	0.002	Dec+Hpf	YD + BA
NH_4^+ †	1624.27 - 1753.3	129.03	0.002		YD + BA
ECM♮	1624.27 - 1753.3	129.03	0.001		YD + BA

Table 6.1: GRIP data used for annual counting in Bølling-Allerød and Younger Dryas. In Younger Dryas only the raw variant of [Ca^{2+}] data were used. In Bølling-Allerød the included [NO_3^-], dust, [Ca^{2+}], [NH_4^+], and ECM profiles were re-sampled to 1 cm resolution. However, for the Younger Dryas section it was possible to include the original data sets of the specified resolution. Ost D denotes Oldest Dryas. ‡Hammer et al. [1997]; Hammer [In press], †Fuhrer et al. [1993, 1996], ♮Taylor et al. [1993].

The measurements of the ion concentrations of Ca^{2+} and NH_4^+ were performed by Fuhrer et al. [1993, 1996] by a continuous melting and continuous flow set-up. The technical resolution of the [NH_4^+] and [Ca^{2+}] profiles is 2 mm. The original data set of 2 mm resolution has been applied for the annual layer counting of the Younger Dryas period, while the data profile was re-sampled to 1 cm for the Bølling-Allerød section, reducing the effective resolution down to 3-4 cm.
Sigfús Johnsen [Pers. comm.] has made two different modifications of the [Ca^{2+}] data, which have been included in the annual counting of the Bølling-Allerød section. One set of the [Ca^{2+}] data has been deconvoluted to correct for mixing in the apparatus during measurements. The transfer function was $\exp(0.1 \cdot f)$, where f

is frequency. The cut-off frequency was 30 cycles m^{-1}, thus the data are able to resolve years of a thickness down to 3.3 cm. It should be mentioned that the deconvolution corrects only the amplitudes of the cycles, not their relative phases. The other variant of the $[Ca^{2+}]$ data has been filtered through a smooth Gaussian high-pass filter, so that the low-frequency oscillations, which are of no interest for annual counting, are damped out.

The dust and NO_3^- concentrations were measured in 1-10 mm resolution on melted ice [Hammer et al., 1997; Hammer, In press]. The dust concentrations were measured by laser and calibrated by a Coulter Counter. The sampling resolution is not constant through the data set as the sampling speed was changed during the data acquisition in field. As is the case for the the ECM and the $[NH_4^+]$ and $[Ca^{2+}]$ profiles, the original dust and $[NO_3^-]$ have been used for the dating of Younger Dryas, while re-sampled profiles of 1 cm have been used for the annual layer counting in Bølling-Allerød.

6.2 δD and δ^{18}O

The new high resolution δD data from the Bølling-Allerød period in the GRIP ice core were presented in Chapter 5. The detailed oxygen isotope record is briefly described in the following. The sampling and the measurements of the new high resolution δ^{18}O data[1] from the GRIP deep core have been performed by Trine Ebbensgaard Strømfeldt, Thore Jürgensen and Anita Boas at the University of Copenhagen, Denmark.

A total of 1485 samples were cut in 1 cm intervals along the ice core and the volume of each sample constituted at minimum 3 cm^3. The δ^{18}O measurements were performed on a mass spectrometer which applies an equilibrium method, where the melted ice samples are equilibrated with CO_2 gas under vibrations. The samples were kept in equilibrium with CO_2 gas at room temperature for 6 hours before the gas was subjected to isotopic analysis. The ratio of mass 46 to 44 in the

[1]The report *Kold Event i Allerød* on the δ^{18}O data can be acquired upon request at the library at the Niels Bohr Institute, Juliane Maries vej 30, 2100 Copenhagen Ø, Denmark.

CO_2 gas is a measure of the $^{18}O/^{16}O$ ratio in the sample. There is no observable inter sample memory connected to this method.

The sampling intervals of the $\delta^{18}O$ series are displayed in Figure 3.2 and Table 6.1. The $\delta^{18}O$ series are named $\delta^{18}O$ Interval I and $\delta^{18}O$ Interval II. It is seen that the stable isotope profiles cover a total depth of 36.85m, of which 1.1m is an overlap between $\delta^{18}O$ Interval II and a part of δD Interval III in early Bølling. The overlapping δD and $\delta^{18}O$ series are from two different cuttings of the ice and they were measured separately[2].

6.2.1 Correction for diffusion

The new high resolution isotope series of δD and $\delta^{18}O$ have been corrected for diffusion in the firn and ice. The methods and techniques behind the reconstruction of the original signal in stable isotope records were presented in Section 4.4. The results of the back diffusion are presented here.

Figure 6.1 and 6.2 show all the intervals of the new high-resolution stable isotope data from Bølling-Allerød in the GRIP ice core. The δ-values are reported relative to the VSMOW-SLAP scale. In Figure 6.1 the measured and the deconvoluted data, which is an estimated reconstruction of the initial isotope profile, are plotted together. It is the reconstructed annual signal that is used for dating, by means of counting the summer peaks of high isotope values, as will be described in Chapter 7. The overlapping section between $\delta^{18}O$ Interval II and a part of δD Interval III is displayed in Figure 6.2, where the measured data are plotted in the upper panel (a) and the deconvoluted data are shown in the lower panel (b). There is good agreement between the two different isotope profiles.

[2]Deuterium excess (d), which is defined as $d = \delta D - 8\delta^{18}O$, has not been calculated as the different cuttings may lead to a false deuterium excess profile.

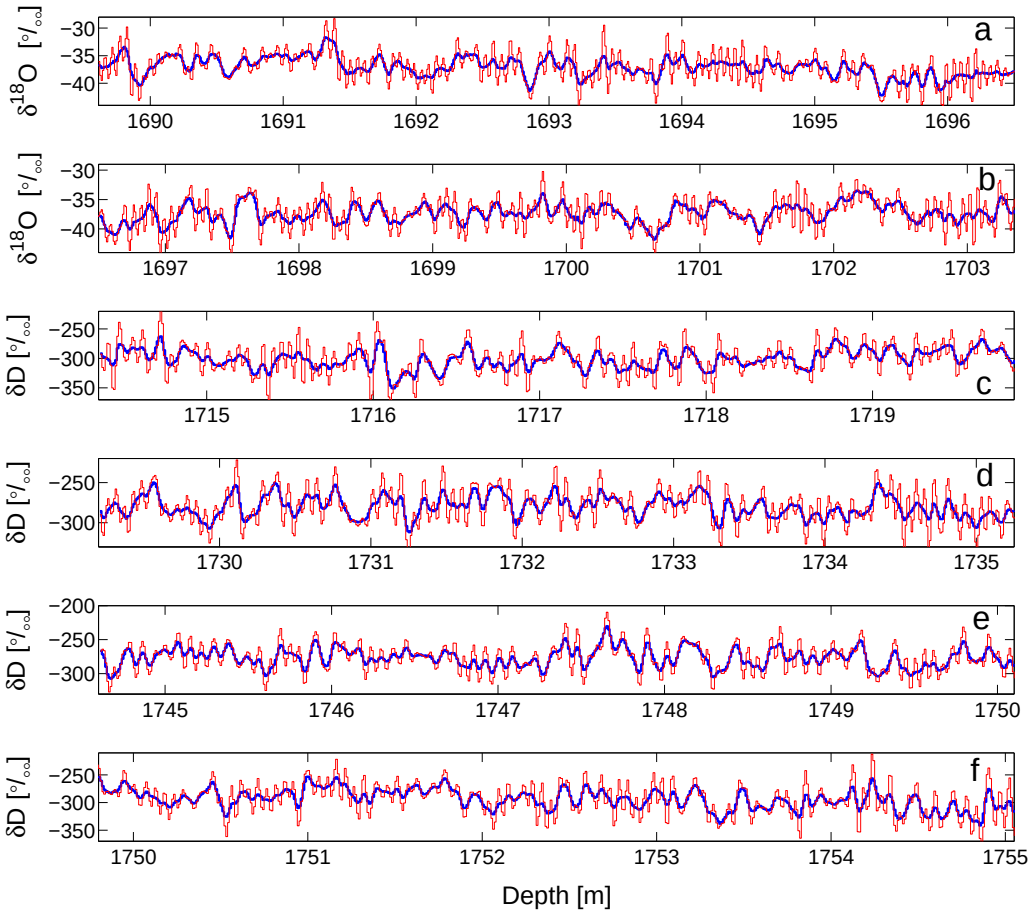

Figure 6.1: Measured (blue) and deconvoluted (red) isotope data. (a,b) δ^{18}O Interval I, (c) δD Interval I, (d) δD Interval II and (e,f) δD Interval III. See Figure 6.2 for δ^{18}O Interval II.

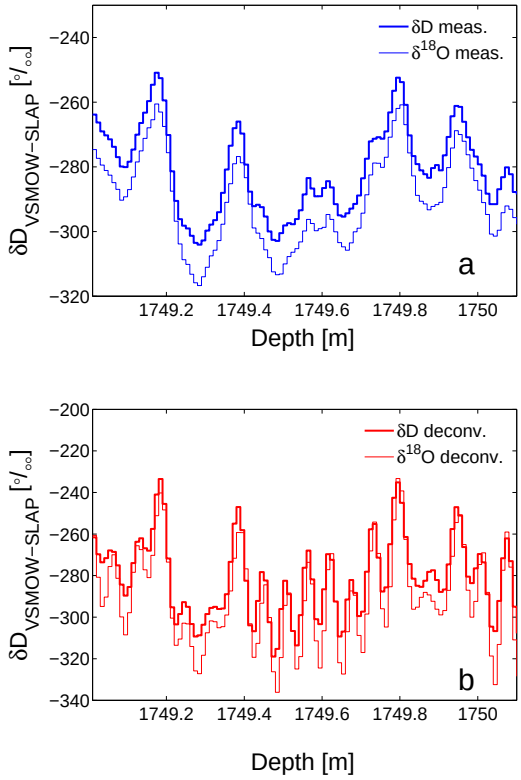

Figure 6.2: Overlapping section of δD (thick) and δ^{18}O (thin). (a) Measured data. (b) Back-diffused data. The δ^{18}O-values are multiplied by 8.

Figure 6.3 displays the MEM power spectra for the isotope intervals presented in Figure 6.1, while Figure 6.4 displays the power spectra for the section where the δ^{18}O and δD profiles overlap. The spectral densities of the δ^{18}O profile have been multiplied with 64 to facilitate the comparison with the spectral densities of the δD section. The power spectra of the measured data (thick lines) show how the amplitudes of high frequencies have been diminished by the diffusion in the firn and ice. The spectral densities in the high frequency domain have been lowered, so that they are indistinguishable from the nearly flat level (white noise) that represents the measuring error (see Table 6.2).

The arrows in Figure 6.3 and 6.4 indicate what is considered as the annual peaks in the power spectra. All the spectra for the measured data reveal an annual peak around 14-20 cycles per meter, which equals an annual layer thickness of 5-7 cm. It is noticed that the annual peak is not very pronounced and that it is situated close to the noise level and therefore close to the cut-off frequency. By comparing the spectra of the measured δD and δ^{18}O in Figure 6.4 in a band around the annual peak, it is observed that the power of δD is higher than for δ^{18}O, relative to that at lower frequencies. In other words, the damping of the annual signal is less for δD than for δ^{18}O. This is in accordance with earlier results and theory [Johnsen et al., 2000] and can be explained by less diffusion of molecules containing D compared to molecules containing ^{18}O. The lower damping of the δD signal suggests that δD is slightly better for dating when working with ice where the amplitude of the annual signal of the stable isotopes is close to the limit of detection.

The thin lines in Figure 6.3 and 6.4 are the power spectra of the back-diffused series. These spectra show how all the frequencies below a certain limit (determined by the cut-off frequency) are amplified to correct for the diffusion. The power density of the annual cycle, which is of interest for dating, has been increased. Table 6.2 lists specifications on parameters that have been used in the MEM spectral analysis and deconvolution of the stable isotope data. The diffusion length σ and the cut-off frequency f_{max} are used for the inverse transfer function $\overline{F}$ as described in Section 4.4 and m is autoregressive order. The choice of cut-off frequency, which is the maximum frequency that is allowed in the back-diffusion, is

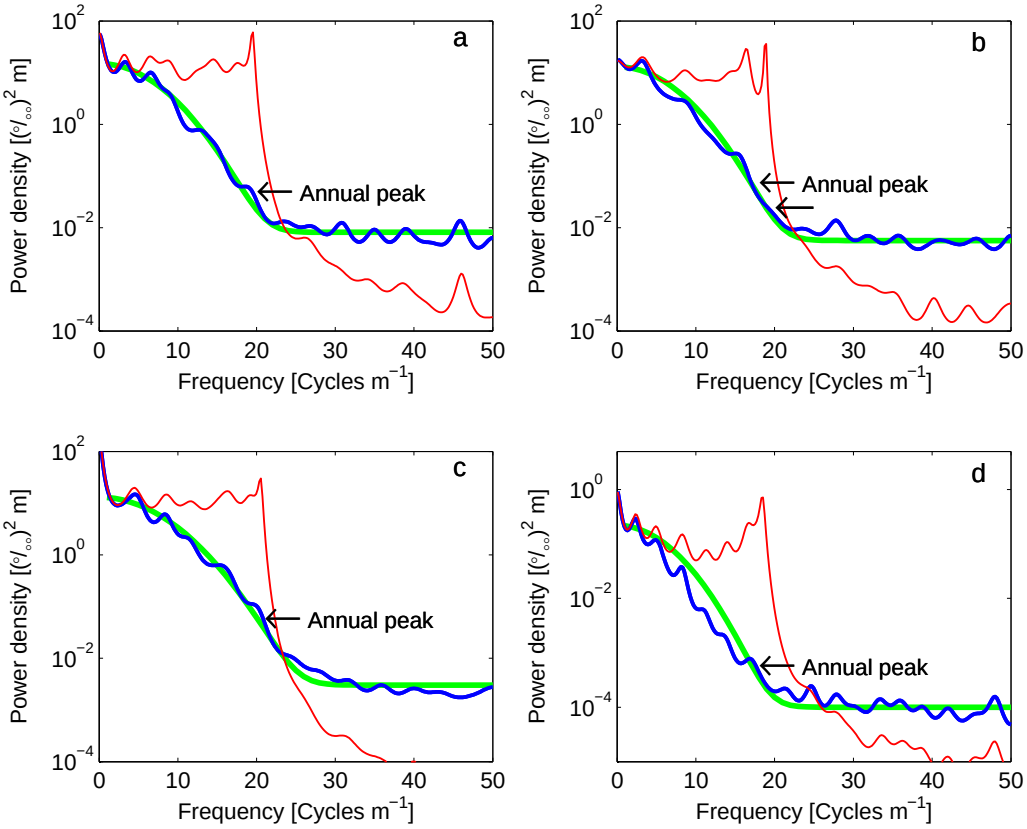

Figure 6.3: MEM power spectra of measured (blue) and deconvoluted (red) isotope data. The diffusion curve (green) reproduces the power densities of the measured series. The arrows indicate what is considered as annual peaks. (a) δD Interval I, (b) δD Interval II, (c) δD Interval III and (d)δ^{18}O Interval I. See Figure 6.4 for δ^{18}O Interval II. See Table 6.2 for a specifi cation of the parameters used in the MEM-analysis.

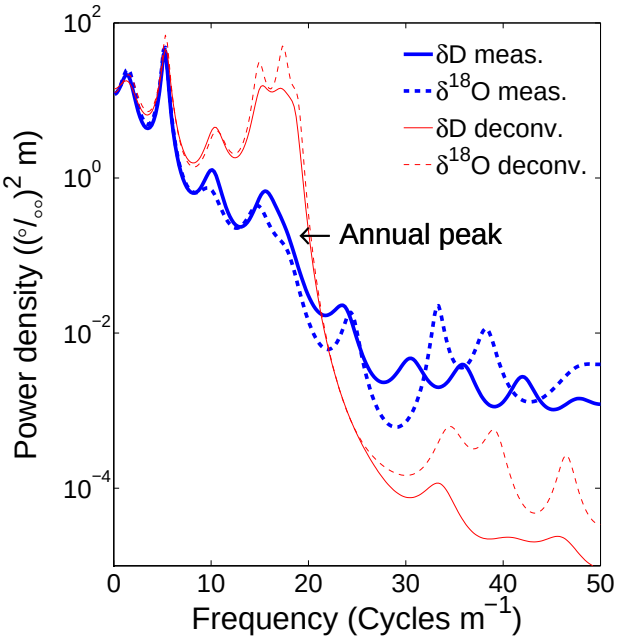

Figure 6.4: MEM spectral densities of overlapping section of δD (solid) and δ^{18}O (dotted). See Figure 6.2. Thick lines = measured data. Thin lines = Back-diffused data. The spectral densities of δ^{18}O are multiplied with 64. In a band around the annual peak there is relatively more power in the δD data compared to the δ^{18}O data.

a best compromise between excluding the noise at higher frequencies and including the annual peak. A f_{max} of $\sim$20 cycles m^{-1} seems to fulfil these conditions for the stable isotope profiles in Bølling-Allerød. This means that back-diffused data are capable of resolving annual layers of a thickness $\geq$5 cm. The right column of Table 6.2 displays the measuring error of the stable isotope series, as revealed in the spectral density plots.

The power spectra reveal a peak around 14-20 cycles m^{-1} for both δD and δ^{18}O, which indicates that there is power left in the annual signal in both of the stable isotope series, and that they can be used for dating purposes. That this peak reflects a true seasonal signal, is confirmed when seeing the good agreement

Interval	σ	m	f_{max}	*Meas. error*
	m		m^{-1}	‰
δD I	0.021	30	20	0.9
δD II	0.0215	30	19	0.75
δD III	0.0185	30	21	0.55
δ^{18}O I	0.023	40	19	0.1
δ^{18}O II	0.021	20	19	0.085

Table 6.2: MEM parameters used in MEM spectral analysis. The filter length was 100 points.

between δD and δ^{18}O in the overlapping section in Figure 6.2. If the peaks in the spectral densities were representing noise only, it would not be possible to create such a compelling agreement between the back-diffused δD and δ^{18}O data, as the noise in the two profiles is uncorrelated. Hence, it is unquestionable that there is power left in the annual amplitude of the stable isotope profiles. What remains to be answered is, if all the years are resolved.

7 Annual layer counting

The high resolution GRIP data that were presented in the previous chapter have been used for annual layer counting in Bølling-Allerød and in Younger Dryas, aiming at estimating the duration of these periods. In the first part of the chapter the steps in the dating process are briefly presented, followed by a description of the applied counting method and how the climate periods Bølling-Allerød and Younger Dryas are defined in this work. Furthermore, the chapter includes a section on how the GRIP record have been matched to the NGRIP record on a detailed scale in the Bølling-Allerød period. The results of the multi-parameter dating of the Bølling-Allerød and Younger Dryas periods in the GRIP ice core are presented in the last part of the chapter. The new results are compared with existing stratigraphical and modelled timescales from the GRIP core and with the new stratigraphical dating of the NGRIP core, as well as with annual layer countings of the GISP2 core.

7.1 Steps in the dating process

The first step of the dating part of this project was an annual layer counting of the GRIP core in Bølling-Allerød giving an estimate of the duration of this interstadial, as presented in Seierstad et al. [In press].
Succeedingly, the Bølling-Allerød section in the GRIP core has been matched on a detailed scale with the NGRIP core, by comparing the [NH_4^+] profiles from the two cores. Using this matching the annual layer counting has been compared with results from the new stratigraphical NGRIP timescale (GICC05).

The last step in the dating process was to include Younger Dryas in the multi-parameter dating. The motivation was to fill the gap between the end of the GRIP part of the new GICC05 timescale and the Bølling-Allerød section of Seierstad et al. [In press], hereby obtaining an independent stratigraphical time scale covering the Younger Dryas and Bølling-Allerød that can be compared with the GICC05 time scale that relies only on annual layer counting using NGRIP data.

7.2 Annual layer counting in Bølling-Allerød

The annual layer counting of Bølling-Allerød has been performed by counting annual cycles in deconvoluted δD, deconvoluted δ^{18}O, [NH_4^+], [Ca^{2+}] (raw, deconvoluted and high-pass filtered), dust concentrations, [NO_3^-] and ECM as listed in Table 6.1 and as seen in Figure 7.1. As described in Chapter 6 the resolution of all the used data series was 1 cm, which for the case of the isotope series equals the original sampling resolution, while the ECM, dust and ion concentration profiles were re-sampled from an original sampling resolution of 1 and 2 mm.
The multi-parameter counting was done manually based on inspection of all the parameters at one time. One “master” series of years has been established from this common interpretation. In Figure 7.1 this master series can be seen as dots on the [NH_4^+] profile. A *certain year* is defined as an annual peak which is clearly seen in all (or most) of the parameters. A certain year is symbolised with a black dot. However, sometimes the cycles may be hard to interpret, e.g. when one series indicates a year where another series does not, or that a possible year is seen as a shoulder on a flank of a peak. These ambiguities lead to *uncertain years* (marked by open dots). The best estimate of the number of years within any depth interval is taken as the number of certain years + half of the number of uncertain years. The uncertainty is taken as half of the uncertain years. This uncertainty reflects the degree of difficulty in identifying the annual peaks in the data, but does not reflect the total uncertainty, as there might be a bias in the dating, e.g. if the data does not resolve all the years, or if years are missing from the precipitation record.

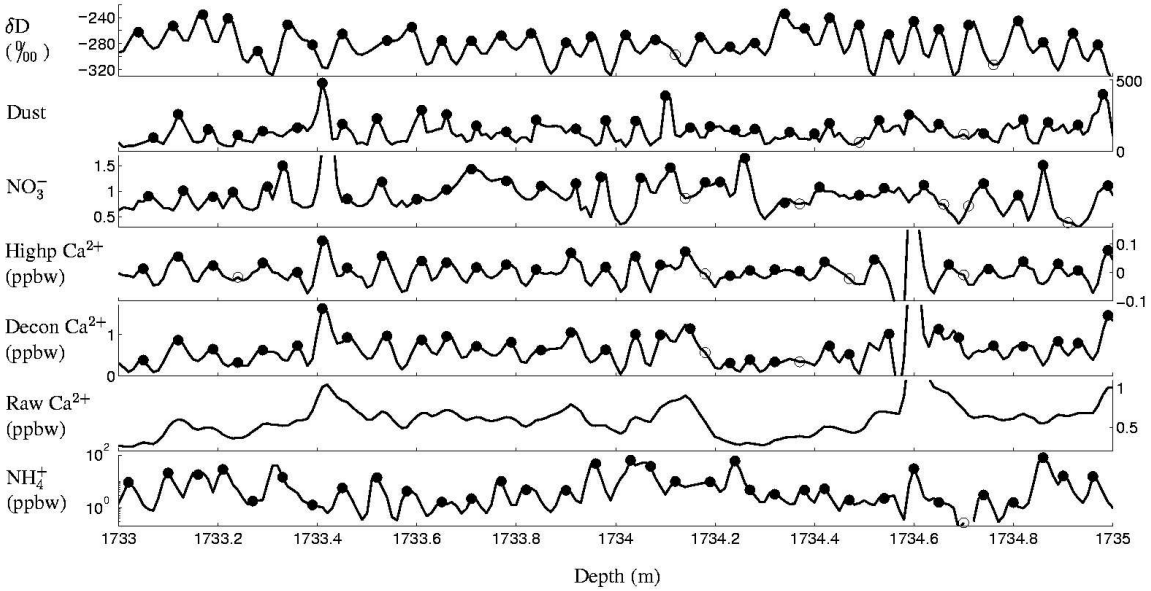

Figure 7.1: Example of multi-parameter dating in Bølling-Allerød. Counting of annual layers is performed on deconvoluted δD (or δ^{18}O), dust concentrations, $[NO_3^-]$, $[Ca^{2+}]$ (high-pass, deconvoluted and raw) and $[NH_4^+]$. A black dot symbolises what is considered to be a certain annual layer, while an open dot represents what is interpreted as an uncertain annual layer. The dots marked in the $[NH_4^+]$ profile constitute the "master" series, as described in the text.. The units on the dust and $[NO_3^-]$ profiles are arbitrary.

The counting was first performed on the sections where all the data were available, i.e. in the intervals where the stable isotopes have been measured, aiming at establishing whether there is an overall agreement between the series. Thereafter, the rest of the Bølling-Allerød period was counted, using the experience that was gained from intervals containing stable isotope profiles.

When comparing the seasonal cycles in the different parameters in Figure 7.1 it is seen that there is good overall agreement between the parameters. $[NO_3^-]$ is the parameter that deviates most from the common behaviour, generally showing less cycles than the other parameters. Within certain sections no weight has

been put on the [NO_3^-] in the interpretation of the seasonal cycles, because it was apparently too smooth. However, in periods [NO_3^-] agrees well with the other parameters. The dust profile often have more peaks than the other parameters, advocating for the highest number of years, while the [NO_3^-] and the stable isotopes generally define the lower limit on the number. The deconvoluted [Ca^{2+}] and [NH_4^+] generally serve as good dating tools. As previously mentioned, dust can have more than one peak within some years. The exclusion of dust peaks which are considered as "double peaks" has been decided by comparison with the seasonal cycles in the stable isotopes, [Ca^{2+}], [NH_4^+] and [NO_3^-].
Under present day conditions [NH_4^+] and [NO_3^-] have maxima during summer like δD and δ^{18}O, while dust and [Ca^{2+}] normally peak during spring. This is also the main behaviour during Bølling-Allerød, though there are periods where this is not the case. The parameters are often drifted away from their usual relative phasing, especially in Allerød. Hence, the seasonality pattern seems to have had a higher variability than under present day conditions.

7.3 Annual layer counting in Younger Dryas

The annual layer counting within Younger Dryas has been performed by including series of ECM, dust concentrations, [NH_4^+], [Ca^{2+}] and [NO_3^-] as seen in Table 6.1. As mentioned in Chapter 6 the data series that were used for the Younger Dryas section had the original sampling resolution of 1 mm and 2 mm, instead of a re-sampled 1 cm resolution, which was the case for the Bølling-Allerød interval.

Suspicions from the annual layer counting in Bølling-Allerød, as presented in Seierstad et al. [In press], that the applied counting method for that period most likely leads to an underestimation of the number of counted years in colder periods with low accumulation, and also knowing that the expected annual layer thickness of around $\sim$3-4 cm in Younger Dryas [Dahl-Jensen et al., 1993; Johnsen et al., 2001] is at the limit of what the data can resolve, the counting approach was

Onset of event	*Depth*	*How defined*		*Depth*$^{\natural}$	*Depth*†
	m	*Parameter*	*Core*	m	m
Bølling	1753.3	Excess	NGRIP	1753.40	1752.85
Older Dryas	1718.6	δD, δ^{18}O	GRIP	-	-
Allerød	1715.0	δD, δ^{18}O	GRIP	-	1718.20
Younger Dryas	1662.4	Excess	NGRIP	1661.55	1662.65
Holocene	1624.27	Excess	NGRIP	1623.60	1623.60

Table 7.1: Depths of the onset of Bølling, Older Dryas, Allerød, Younger Dryas and the Holocene in the GRIP ice core, as used in this work (left) and in previous works (right, $^{\natural}$Johnsen et al. [1992a], †Hammer et al. [1997]). Column 3 and 4 specify which parameters from which core that have been used in this work to define the depths of the onset of the events. Excess = deuterium excess. See text for further explanation.

changed slightly for the Younger Dryas section. The condition of an *overall agreement* between the series for defining a certain year was relaxed, so that an annual layer could be interpreted as *certain* on the basis of an observed cycle in one parameter, only. This means that if one of the data series shows a clear annual cycle, while the other series are smoothed out this is treated as a certain year. Uncertain annual layers are used if none of the series have a clear annual cycle, but some of them indicate a year by having a shoulder on a peak.
The annual layer counting in the Younger Dryas section was performed in collaboration with Bo Vinther.

7.4 Definitions of depths of transitions

Defining the exact depths of the onset and termination of a climate period observed in ice core records is not always straightforward, as the different data series may show a slightly different behaviour, e.g. in timing and rate of change, across a

climate transition. In the following the depths used in this project are presented. The left part of Table 7.1 displays the depths of the onset of the climatic periods Bøling, Older Dryas, Allerød, Younger Dryas and Holocene that have been used in this project. The definition of the onset of Bølling, Younger Dryas and Holocene are all based on sharp shifts seen in the deuterium excess profile in the NGRIP ice core [T. Popp, Pers. comm.], as is also the case for the definition of the same climatic transitions in the GICC05 timescale. Deuterium excess, which reflects the conditions in the source area for the moisture [Merlivat and Jouzel, 1979; Johnsen et al., 1989], is characterised by abrupt shifts at transitions from one climate period to another. Hence, this parameter is useful for defining the onset and terminations of the climate periods. The deuterium excess is not available from the depths of interest in the GRIP core, which is the reason for using the NGRIP deuterium excess profile. The NGRIP depths of the transitions are transferred to GRIP depths by matching profiles of ECM, DEP, $[Ca^{2+}]$, $[NH_4^+]$ and $\delta^{18}O$ from the two ice cores. The depths of the onset of Bølling, Younger Dryas and Holocene differ slightly from those defined in [Johnsen et al., 1992a], which were based on ECM and from those defined by Hammer et al. [1997] (see right part of Table 7.1).
The definition of the onset of Older Dryas and Allerød are defined by shifts seen in $\delta^{18}O$ and the new δD data in the GRIP ice core. Neither of these depths have been defined in [Johnsen et al., 1992a]. Hammer et al. [1997] did not specify the depth interval of Older Dryas and their depth of the onset of Allerød almost coincides with the depth of the onset of Older Dryas used in this work. In the new stratigraphical dating of the NGRIP core the depths of the Older Dryas period are not specified.

7.5 Matching GRIP and NGRIP in Bølling-Allerød

The GRIP and NGRIP records have been matched on a detailed scale within the Bølling-Allerød period. First, a few fix points were obtained by matching characteristic large scale peaks of ECM, DEP and $[Ca^{2+}]$ from the two cores and also by using newly observed tephra layers of chemically identical composition

in the two cores [Mortensen et al., 2005, In preparation; S. Davies, Pers. comm.]. These coarsely spaced fix points define sections within which one can zoom to look for similar patterns in the corresponding data series of the two cores. As is the case for the Holocene part of the GRIP and NGRIP cores, the [NH_4^+] profiles are excellent for high resolution matching [Rasmussen et al., Submitted]. The similarity between the GRIP and NGRIP [NH_4^+] profiles is striking and within sections of a few meters it is possible to match the profiles on an annual scale. The profiles show similarities both in amplitude and in wavelength. Almost 700 matching points between GRIP depths and NGRIP depths have been found in Bølling-Allerød. The fix points are displayed in Figure 7.2. The detailed matching of the two cores provides a basis for a comparison of the annual layer counting of Bølling-Allerød in this work with the new stratigraphical dating of the NGRIP core [Rasmussen et al., Submitted], which is made by identification and counting of annual cycles as observed in impurity records measured in a continuous flow system [Röthlisberger et al., 2000; Bigler, 2004].

So far, the matching of the two cores has been restricted to the Bølling-Allerød period, but an initial investigation shows that it it possible to match the [NH_4^+] profiles in Younger Dryas as well, which is promising for further comparison of the GRIP and the NGRIP timescales in this period.

7.6 Results and discussion

The estimated duration of Bølling, Older Dryas, Allerød and Younger Dryas derived from the annual layer counting based on seasonal variations in δD, δ^{18}O, [NH_4^+], [Ca^{2+}] dust concentrations and [NO_3^-] in the GRIP core are listed in Table 7.2. In Table 7.3 these results are displayed along with other duration estimates of the same periods from the GRIP core and from other deep ice cores drilled in Greenland.

The annual layer thickness λ for each of the periods derived from the multi-parameter dating is displayed as mean values for the listed periods in Table 7.2.

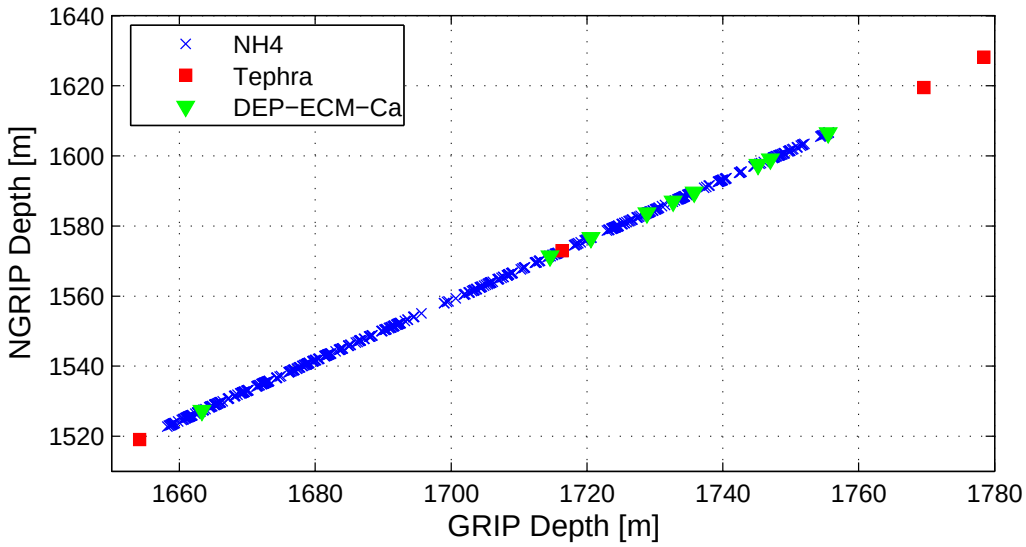

Figure 7.2: Fix points between the GRIP and NGRIP cores in the Bølling-Allerød section.

Annual layer thicknesses in 2 m averages are displayed in panel a of Figure 7.3. For comparison the modelled annual layer thickness based on the ss09sea timescale is also shown in the plot [Johnsen et al., 2001; Johnsen, Pers. comm.]. The ss09sea timescale is based on a Dansgaard-Johnsen flow model and δ^{18}O-derived accumulation rates.

When comparing the results from this work with the existing stratigraphical dating of the GRIP ice core [Hammer et al., 1997; Hammer, In press], it is seen that the number of years within the Bølling-Allerød interval is substantially lower for the multi-parameter approach, while the two estimates of the duration of Younger Dryas agree within the margins of the uncertainty. As mentioned in Section 7.4 the Older Dryas period was not specified in the work by Hammer et al. [1997]. By using their depths for the Bølling and Allerød intervals, the corresponding estimates for the multi-parameter approach are the following: Bølling: 587 ± 16 and Allerød: 1028 ± 34. These estimates are $\sim$20% and $\sim$30% shorter than those found by Hammer et al. [1997]. The highly significant deviation between the two

Period	*Number of annual layers*		*Duration*	λ	*Ratio of duration*
	Certain	*Uncertain*	yr	cm	GRIP/NGRIP
Bølling	571	33	588±16	5.9	0.96±0.04
Older Dryas	66	8	70±4	5.1	0.78±0.06
Allerød	939	63	971±31	5.4	0.89±0.04
Younger Dryas	1106	88	1150±44	3.3	0.96±0.05

Table 7.2: Estimated duration of Bølling, Older Dryas, Allerød and Younger Dryas and the corresponding mean annual layer thickness (λ) in the GRIP ice core from the multi-parameter dating in this work. The duration is defined as the number of certain annual layers + half of the numbers of uncertain annual layers. The uncertainty on the duration is half of the numbers of the uncertain annual layers. The uncertainty reflects the inconsistency between the annual signal in the series and the difficulty of interpreting the peaks and shoulders. The uncertainty does not take into account any bias in the counting, or imperfections of the annual layer sequence itself. The right column shows the ratio of the duration in the GRIP core to the duration of the corresponding period in the NGRIP core, based on the GICC05 timescale [Rasmussen et al., Submitted].

stratigraphical annual layer counts on the same core can be explained by the different ways of performing the layer counting. The method that has been used for the Bølling-Allerød interval in this study may have underestimated the duration of the climate periods, as a high degree of agreement of the data series was required to define a certain annual layer. In this way, the result is highly dependent on the resolution and the internal consistency of the data series included in the annual layer counting. As described in Section 7.2, the [NO_3^-] and the stable isotopes often define the lower limit on the number of certain annual layers, and as will be presented later in this section, detailed comparison with the NGRIP core supports what the spectral analysis of the δD and δ^{18}O series indicated, namely, that the stable isotopes series are not able to resolve all annual layers within sections of

low accumulation in Allerød and Older Dryas. This is also supported by the fact that shoulders are seen on flanks of δ-peaks where other parameters have peaks (or clear shoulders).
On the other hand, the dating performed by using dust concentrations only without support from other parameters may have overestimated the number of years, by assigning two annual marks to "double peaks" that only represent one year. Also the observed variability in seasonality within the Allerød section, suggests that multiple data series are necessary when interpreting the peaks in the dust profile.

Compared with the modelled time scale ss09sea it is seen that the annual layer thickness from the multi-parameter dating corresponds well with the modelled results through most of the Bølling period and in the Younger Dryas section. However, in the Younger Dryas section the decreasing trend in the modelled layer thickness with depth is not supported by the observed λ values. Comparison of the annual layer thickness in the NGRIP core by Rasmussen et al., [Submitted] with the ss09sea timescale for the NGRIP core shows that the decreasing trend in λ is seen in both modelled and observed results. This indicates that an annual layer thickness of 3 cm might be the lower limit of what the GRIP data from the Younger Dryas section can resolve. Further work on extending the detailed matching of [NH_4^+] profiles from the GRIP and the NGRIP core through the Younger Dryas will hopefully shed light on this. The Older Dryas and Allerød durations from the multi-parameter approach are $\sim$21% and $\sim$17% shorter, respectively, compared to the modelled estimates. The highest discrepancies are found in the cold spells (with corresponding low accumulation). This feature is also seen when comparing with the NGRIP timescale GICCO5. In panel b of Figure 7.3 the GRIP/NGRIP ratio of the duration of corresponding depth intervals is graphically displayed through the whole Bølling-Allerød interval. In this plot characteristic fix points at intervals of $\sim$1-3 meters have been selected in order to compare the number of annual layers in corresponding sections in the two cores. The dotted horizontal line represents a ratio of 1. The coloured areas are inserted to mark the depth intervals of the high resolution stable isotope series that have

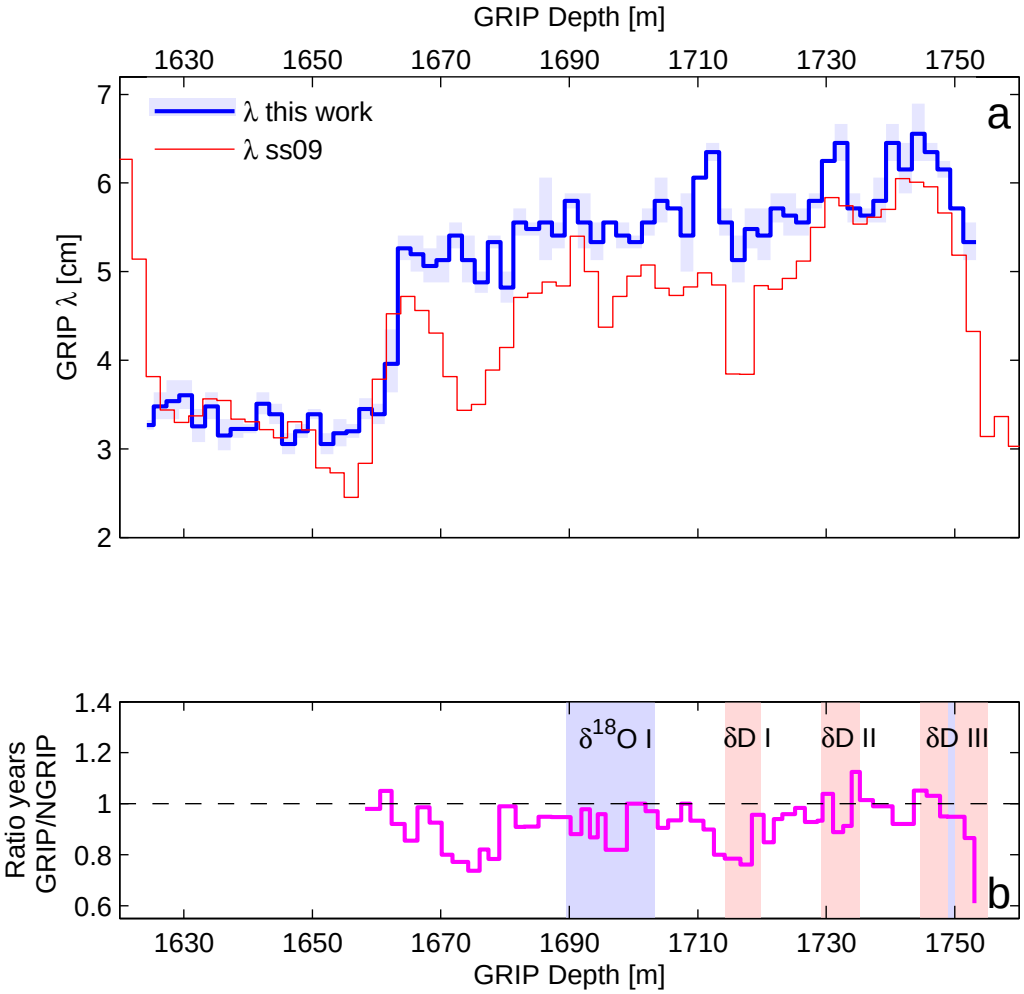

Figure 7.3: (a) Annual layer thickness λ in Bølling-Allerød and Younger Dryas in the GRIP ice core derived from annual layer counting in this work (blue, 2 m averages) and from the age model ss09sea (red, 4 bag averages) [Johnsen et al., 2001, Johnsen, Pers. comm.]. (b) Ratio of the duration in the GRIP core (this work) to the duration in the NGRIP core (GICC05 timescale, Rasmussen et al. [Submitted]) of corresponding depth intervals. Matching the depth of the two cores has been done by using $[NH_4^+]$ profiles as described in Section 7.5. In this plot selected matching points have been used to calculate the ratio of the duration from one fix points to the other. The dotted line represents an equal amount of observed annual layers in the two cores. Light red areas = δD interval I, II and III. Light blue areas = δ^{18}O interval I and II (the latter is the thin blue area within δD Interval III).

Core	*Method*	*B* yr	*OD* yr	*A* yr	*YD* yr
GRIP	$[Ca^{2+}]$, $[NH_4^+]$, dust, δD, δ^{18}O,ECM, $[NO_3^-]$	588±16	70±4	971±31	1150±44
GRIP	Dust[†]	736	-	1432	1194
GRIP	Modelled (ss09sea)[♭]	640	89	1170	1183
NGRIP	CFA-data[♮]	614±16	90±1	1091±29	1193±39
GISP2	Ice layer count[‡]	580±29	80±4	1120±56	1240±62

Table 7.3: Estimates of the duration of Bølling (B), Older Dryas (OD), Allerød (A) and Younger Dryas (YD) from deep ice cores from Greenland. The duration estimates based on the ss09sea timescale are calculated by using the depth intervals as defined in this work (left part of Table 7.1). This is also the case for the duration estimates from the NGRIP stratigraphical dating, where the GRIP and NGRIP depths are matched as described in Section 7.4. The duration estimates based on dust countings in the GRIP core are given with the depths specified by Hammer et al. [1997] (right column of Table 7.1). A rough comparison of the results from the multi-parameter approach and the dust countings can be done by comparing the sum of the duration of Allerød and Older Dryas estimated from multi-parameter approach with the Allerød duration from Hammer et al. [1997]. The results from the GISP2 datings are given as reported in [Stuiver et al., 1995]. Comparison of the δ^{18}O profiles from GRIP [Johnsen et al., 1997] and GISP2 [Stuiver et al., 1995; The Greenland Summit Ice Cores CD-ROM, 1997] shows that any deviation of the definitions of the onsets and terminations of the periods is not of significance compared to the uncertainty in the dating. The uncertainty on the stratigraphical dating of the GISP2 core at this depth is 5% [Alley et al., 1993]. [†]Hammer et al. [1997]; Hammer [In press], [♭]Johnsen et al. [2001], [‡]Stuiver et al. [1995]; Meese et al. [1997]; Alley et al. [1997], [♮]Rasmussen et al. [Submitted]; R¨othlisberger et al. [2000]; Bigler [2004].

been included in the annual layer counting in the GRIP core. Table 7.4 lists the number of observed annual layers within the sections of high resolution stable isotope in the GRIP core and the number of counted years in the corresponding

sections of the NGRIP core. The ratio of number of years in the GRIP core to the number years in NGRIP core is close to 1 in Bølling, while it is less than 0.8 in Older Dryas and in the cold spell at the end of Allerød. The ratio reaches its minimum of $\sim$0.6 at the transition from Oldest Dryas to Bølling.

According to data from Dahl-Jensen et al. [1993] the mean accumulation rate (based on δ^{18}O measured in the ice) at GRIP in Bølling was 0.23$\pm$0.02 myr^{-1}, while it was 0.15$\pm$0.02 myr^{-1} in Older Dryas and 0.18$\pm$0.02 myr^{-1} in Allerød. As 0.20 myr^{-1} is considered to be the minimum accumulation rate under present day conditions for the annual cycle in stable isotope profiles to survive firnification [Johnsen, 1977], it is not surprising that the stable isotope sections (δD II, δD III Bølling part and δ^{18}O II) within the Bølling interval successfully seem to resolve all or most annual layers. The lower modelled accumulation rates for Older Dryas and Allerød could explain why the number of annual layers within the stable isotope sections (δ^{18}O I and δD I) from these two climate periods is less than in the corresponding NGRIP sections. One could speculate whether it would be possible to retrieve the apparently lost layers in the isotope profiles by cutting ice samples of higher resolution than the 1 cm resolution which has been done in this project. The spectral analysis of the δ^{18}O and δD intervals and the comparison with seasonal cycles observed in the chemical parameters during the dating process show that there is power left in the annual signal in both of the stable isotope series. However, some years of low accumulation (corresponding to high frequency) may not be revealed by the deconvolution, as they are hidden in the noise and thereby ruled out by the cut-off frequency. With a cut-off frequency of $\sim$20 cycles m^{-1}, annual layers with a thickness less than $\sim$5 cm will not be resolved. It is interesting that it is possible to detect the annual amplitude at all within the stable isotope series from Older Dryas and Allerød. This can either be explained by higher accumulation rates than those derived from δ^{18}O, or by lower temperatures compared to present, because the weakening of the amplitude is highly temperature dependent. δ^{18}O derived paleotemperatures [Johnsen et al., 1995] from the GRIP ice core shows that it was only 1 °C colder during Bølling compared to today, while it was 5-12 °C colder during Older Dryas and Allerød.

Interval	*Duration* [yr]		*Ratio of duration*
	GRIP	*NGRIP*	*GRIP/NGRIP*
δ^{18}O I	251±6	276±10	0.91±0.04
δ^{18}O II	18±0	20±0	0.90±0
δD I	103±5	128±2	0.80±0.05
δD II	99±1	100±3	0.99±0.03
δD III	181±3	209±6	0.87±0.03
δD III Bølling part	149±2	155±5	0.96±0.03
δD III Oldest Dryas part	33±1	55±1	0.60±0.03

Table 7.4: A comparison of observed annual layers within the high resolution stable isotope sections in the GRIP core (this work) and the corresponding depth intervals in the NGRIP core (GICC05, Rasmussen et al. [Submitted]). The interval δD III spans the the termination of Oldest Dryas and the beginning of Bølling. The two bottom rows display the Bølling part and the Oldest Dryas part, respectively. It should be mentioned that the matching of the two cores around the interval δ^{18}O II is uncertain. The two year difference between the GRIP dating and the NGRIP dating of this section may arise from uncertain matching.

The estimate of the duration of Bølling agrees well with the number of years found by annual layer counting of the GISP2 ice core [Alley et al., 1993, 1997; Stuiver et al., 1995; Meese et al., 1997]. The estimated durations of Older Dryas and Allerød are $\sim$13% shorter than those from the GISP2 layer counting, and the Younger Dryas estimate is 7% shorter.

To summarise, the duration estimates of the Bølling and Younger Dryas periods from the multi-parameter layer counting in the GRIP ice core agree well with the new NGRIP stratigraphical dating and previous estimates from the GRIP core, while the estimates of Older Dryas and Allerød are significantly shorter compared to the other datings as seen in Table 7.3. There might be several explanations to

why the durations of the Older Dryas and Allerød sections seem to be underestimated. One explanation is that the applied counting method and the resolution of the data series were different for the Younger Dryas section and the Bølling-Allerød section. Within the Bølling-Allerød section the annual layer counting was first performed in the intervals where the stable isotopes data are available, based on the assumption that the stable isotopes would give a representative estimate of the number of annual layers. The experience from the counting of these sections was used while counting the remaining parts of the Bølling-Allerød. When interpreting the cycles in the different data series, a high degree of agreement between the different series was required to define a certain annual layer. This condition implies that the result is highly dependent on the resolution of the data series with the lowest resolution and the internal consistency of the data series. Furthermore, the observed variability in the seasonality pattern in the Allerød section may have made the interpretation of the cycles in the different data series more uncertain, compared to the more climatic stable Younger Dryas and Bølling periods. Comparison of corresponding sections in the GRIP and the NGRIP cores in panel b of Figure 7.3 and Table 7.4 suggests that this counting approach fails to resolve all annual layers within sections of low accumulation. Initial comparison with the NGRIP record on annual scale, also based on the [NH_4^+] matching, indicates that many of the uncertain annual layers in the GRIP multi-parameter dating should be interpreted as certain annual layers, if the two timescales should be made to match. Further work on the comparison with the NGRIP timescale will hopefully give valuable information for the interpretation of both records.

By including data series with the original sampling resolution of 1 and 2 mm in the Younger Dryas section, instead of the re-sampled 1 cm resolutions series, the interpretation of the seasonal cycles has apparently become more certain. Furthermore, the applied counting method was less restrictive compared to the method used in the Bølling-Allerød interval, i.e. some of the features that would have been defined as uncertain annual layers according to the counting method applied within the Bølling-Allerød section were defined as certain annual layers within

the Younger Dryas section. Even though the annual layer thickness is significantly lower within the Younger Dryas section compared to the rest of the investigated interval, the resolution of the used data series, the applied counting method, and also the relatively stable climate conditions have made the interpretation of the data series easier and more certain.

8 Conclusion

In this study high resolution series of δD have been measured in three depth intervals within the Bølling-Allerød period in the GRIP ice core. These three sections and two high resolution series of previously measured δ^{18}O data have been corrected for diffusion in the firn and ice by applying deconvolution techniques. The deconvoluted isotope profiles have been used for annual layer counting in the Bølling-Allerød period. Seasonal cycles have been identified and counted using isotope data and previously published profiles of ECM, [Ca^{2+}], [NH_4^+], [NO_3^-] and dust concentration, existing for the whole interval. A multi-parameter dating has also been performed in the Younger Dryas section, by counting annual layers observed in series of dust and ion concentrations and ECM from the GRIP core. A detailed matching of the GRIP and the NGRIP records has been performed by matching similar patterns in the ECM and the [NH_4^+] profiles of the two cores, making a comparison with the new NGRIP stratigraphical time scale (GICC05) possible.

The new high resolution isotope data presented in this study shows that it is possible to use stable isotopes for stratigraphical dating of glacial ice from Bølling-Allerød (Greenland Interstadial 1). The annual cycle is seen in MEM power spectra and the cycles of the stable isotopes compare well with the annual cycles in the chemical data series and the seasonal variations in the dust concentrations. It is, however, necessary to deconvolute the measured isotope profiles to reconstruct the initial isotope signals. The maximum resolution of the deconvoluted stable isotope data from Bølling-Allerød is $\sim$5 cm, so annual layers of

less thickness will not be resolved by these data. This implies that some years are lost in colder periods having lower accumulation rates, especially within the Older Dryas and the Allerød periods. This study also confirms the findings of Johnsen et al. [2001] that the dampening of the annual cycle's amplitude, due to diffusion in the firn and ice, is stronger for δ^{18}O than for δD. This suggests that δD is better suited for dating than δ^{18}O when working on ice where the annual signal in the data is weak.
That the amplitudes of the annual signal in the δD and δ^{18}O profiles are detectable, suggests that the annual accumulation rate during the Bølling-Allerød period was not much below 0.20 m ice per year. With a lower accumulation rate, it would be less likely that the annual signal would have survived the diffusion processes in the firn and ice [Johnsen, 1977].

The estimated durations of the Bølling (GI 1e), Older Dryas (GI 1d), Allerød (GI 1abc) and the Younger Dryas (GS 1) periods based on the multi-parameter layer counting in the GRIP ice core are 588$\pm$16, 70$\pm$4, 971$\pm$31 and 1150$\pm$44 years, respectively. The uncertainties reflect the difficulty of the interpretation of the available data and do not take into account any bias in the dating, or imperfections of the annual layer sequence itself. The estimates should be considered as lower limits for these climate periods, as some years may not have been resolved by the data in colder periods with lower accumulation, especially within Older Dryas and Allerød.
This study underlines the importance of having high resolution data when performing stratigraphical dating of ice cores, and having a variety of independent parameters showing seasonal variations.

8.0.1 Outlook

The successful matching of the GRIP and NGRIP records in the Bølling-Allerød section was used in this study to compare the number of observed annual layers in corresponding depth sections of the two cores. Initial investigation indicates

that the matching of the two cores can be extended through the Younger Dryas section. Furthermore, initial investigation of the Bølling-Allerød section shows that it is possible to make a year-to-year comparison of the presented dating with the NGRIP annual layer counting. Further work should establish whether the two timescales can be tied together across the Bølling-Allerød and Younger Dryas periods. Hopefully, the detailed comparison will also reduce the uncertainty on the dating.

A

The duration of the Bølling-Allerød period (Greenland Interstadial 1) in the GRIP ice core

INGER K. SEIERSTAD[1], SIGFÚS J. JOHNSEN[1], BO M. VINTHER[1], JESPER OLSEN[2].

[1] *Department of Geophysics, University of Copenhagen, Juliane Mariesvej 30, DK-2100 Copenhagen Ø, Denmark*

[2] *Department of Physics and Astronomy, University of Århus, Ny Munkegade, DK-8000 Århus C, Denmark*

Abstract

A new dating of the Bølling-Allerød period (Greenland Interstadial event 1) in the GRIP ice core is presented. Newly measured profiles of δD and δ^{18}O, as well as existing profiles of Ca^{2+}, NH_4^+, dust and NO_3^- have been used for the dating. As seasonal variations can be observed in all six components, it was possible to simultaneously count annual layers in the profiles in order to obtain a multi parameter dating. The new data presented in this study includes a total of 36.85 m of stable isotope profiles of 1 cm resolution from 5 sections of the Bølling-Allerød period in the GRIP ice core. The annual layer counting suggests a duration of the complete Bølling-Allerød period, as revealed in the GRIP ice core, of 1627$\pm$52 years. This estimate contrasts an earlier finding from the same GRIP ice core,

where Bølling-Allerød was found to span 2168 years (Hammer and others, 1997; Hammer, in press). This estimate was based on layer counting, using dust concentrations only.

Introduction

The 3028 m long GRIP (GReenland Ice Core Project) ice core was drilled in 1989-1992 at Summit (72 ° 34'N 37 ° 37'W) in Greenland (GRIP members, 1993). The Bølling-Allerød period (Greenland Interstadial 1) is found more than half way down through the ice sheet, at a depth of ∼1700 m, where the annual layer thickness is about 4-6 cm.
The GRIP ice core constitutes a continuous archive of snow and ice, which gives information of past climate in Greenland back to ∼120 000 years BP. Precise dating of the ice core is essential to gain knowledge of climate variability through time. The stratigraphical dating of the GRIP ice core is based on annual layer counting using δ^{18}O, Ca^{2+} and NH_4^+ profiles back to the transition between the last glacial period and the Holocene (Fuhrer and others, 1993, 1996; Johnsen and others, 1999). For older ice, counting has been performed on seasonal variations of dust concentrations back to 60 000 years BP (Hammer and others, 1997; Hammer, in press; The Greenland Summit Ice Cores CD-ROM, 1997). Modelled time scales are available down to the Eemian (Johnsen and others, 2001).

The annual counting of dust concentrations has given estimated durations of the Bølling and Allerød of 1432 and 736 years, respectively (Hammer and others, 1997; Hammer, in press). As dust is brought to Greenland by storms, peaks in dust are, however, likely to represent depositional events, rather than annuality. Due to this, dust may show "double peaks" within one year. When having only this parameter for dating, there is therefore a risk of overestimating the number of years. Motivated by this fact, this study was set up to include as many independent parameters as possible in the dating, all measured in high-resolution and showing

seasonal variations. These parameters include Ca^{2+} and NH_4^+ (Fuhrer and others, 1993, 1996), dust and NO_3^- (Hammer and others, 1997; Hammer, in press) existing for the whole period of investigation, and new sections of δD and δ^{18}O. The main focus has been on the stable isotope profiles, as they are known to be ideal tools for dating ice cores under favourable conditions. They show a strong seasonal cycle, with high values during summer times and low values during winter times. However, diffusion of isotopes in the firn and ice leads to a smoothed isotope profile as time goes by (Johnsen, 1977; Johnsen and others, 2000). Hereby the vulnerable annual cycle is weakened at greater depths. The diffusion process in the firn is dependent on temperature and annual accumulation rates. For the annual cycle to survive the densification process in Greenland the annual accumulation rate has to be greater than $\sim$0.2 m ice per year (Johnsen, 1977). At present at the GRIP site, the accumulation rate is $\sim$ 0.23 m ice per year and the average annual temperature is -32 $^\circ$C (Johnsen and others, 1992).
Until now, stable isotopes have not been used as a dating tool within the glacial period, partly because of low accumulation during glacial times, which speeds up the smoothing of the isotope profile, and partly because of the thin annual layers, which require a high sampling rate. The interstadial Bølling-Allerød was characterized by a relatively warmer climate and a higher accumulation rate compared to the rest of the glacial period (Johnsen and others, 1995), which is promising for retaining the annual cycle. The hope is that this study will enlighten whether it is feasible to use stable isotopes for dating purposes within the Bølling-Allerød interstadial.

New data presented in this study is high-resolution (1 cm) δD and δ^{18}O profiles, from sections of the Bølling-Allerød interstadial in the GRIP ice core. The stable isotope series are sampled from a depth of $\sim$1700 m. There are 3 intervals of detailed δD, covering a total of 22 m of ice, and 2 intervals of δ^{18}O, covering 14.85 m of ice (Table 1, Figure 1). The stable isotope profiles have been deconvoluted to correct for diffusion in the firn and ice. The aim of this study is to investigate if it is possible to retrieve the annual signal in the isotope data from

this depth of the GRIP core and, if so, to estimate the duration of the interstadial Bølling-Allerød, by counting annual cycles in these new data together with annual cycles seen in available high-resolution series of Ca^{2+}, NH_4^+, NO_3^- and dust.

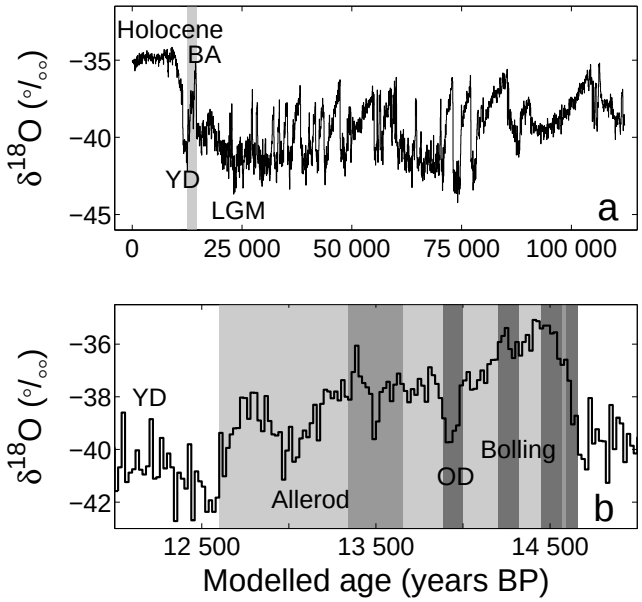

Fig.1. $\delta^{18}O$-profiles on a modelled time scale (ss09sea), where BP=1990 (Johnsen and others, 2001). (a) 50 year averages of $\delta^{18}O$. Bølling-Allerød (BA, light grey band) is the last interstadial (GI event 1) before the cold Younger Dryas (YD) and the subsequent warming in the Pre-Boreal of Holocene. (b) Zoom of the interval which is subjected to investigation (coloured area), 20 year averages of $\delta^{18}O$. The three dark grey bands indicate the intervals, where ice has been sampled and analysed for δD in high resolution to retrieve annual layers and improve the dating of the climate period. The two medium dark areas show the intervals where detailed $\delta^{18}O$ has been included in the dating. Please note that the deepest $\delta^{18}O$-series overlaps a 1.1 m section of the deepest δD-interval. See Table 1 for the depth intervals of the stable isotopes sections. OD = Older Dryas.

Data

A total of 2200 ice samples were cut for δD measurements. The ice, which has been stored at -26 °C, was cut in 1 cm pieces along the ice core, each sample constituting a total volume of $\sim$2 cm^3. The relative abundance of the stable hydrogen isotopes (^{2}H and ^{1}H) was measured on a Micromass (now GV Instruments) continuous-flow Isotope Ratio Mass Spectrometer (CF-IRMS) (Morrison and others, 2001) configured for a chromium reduction technique, using 0.3-0.5 μlitre of each melted sample. The isotopic ratios have been corrected for the production of $^1H_3^-$-ions and the raw δD values (expressed relative to the reference gas) have been corrected for possible drift through the run and for a minor inter sample memory effect. As a last step, the values have been expressed relative to VSMOW and normalised to the VSMOW-SLAP scale (Coplen, 1988; IUPAC, 1994; Nelson, 2000). The average normalisation constant was 1.017.

The δ^{18}O samples were cut in 1 cm pieces and the volume of each sample constituted at minimum 3 cm^3. The δ^{18}O measurements were performed on a mass spectrometer which applies an equilibrium method, where the melted ice samples are equilibrated with CO_2-gas under vibrations. The samples were kept in equilibrium with CO_2-gas for 6 hours before the gas was subjected to isotopic analysis. The ratio of mass 46 and 44 is a measure of the O^{18}/O^{16} ratio in the sample. A total of 1485 samples were measured. T. Ebbensgaard Strømfeldt, T. Jürgensen and A. Boas did the sampling and the measurements of the δ^{18}O data at the University of Copenhagen, Denmark.

To be able to use the annual signal in the isotope series for dating, a deconvolution technique (Figure 3 and 4) has been used to enhance the annual amplitude, which has been weakened through diffusion processes in the firn and ice (Johnsen, 1977; Johnsen and others 2000). The diffusion process can be mathematically described as convolving the initial (unknown) isotope profile with a symmetrical Gaussian clock of the form $\exp(-0.5 \cdot z^2/\sigma^2)$, where the diffusion length σ reflects the degree of smoothing and z is depth. The diffusion length represents the

mean vertical movement of the water molecules and this parameter is dependent on the depth, accumulation rate and temperature. The initial isotope profile can be reconstructed by performing the inverse process (deconvolution) on the measured isotope profiles. MEM (Maximum Entropy Method) analysis is used for calculating the power spectra of the series for estimating the σ to be used (Figure 5, Table 2)

The measurements of the ion concentrations of Ca^{2+} and NH_4^+ were performed by Fuhrer and others (1993,1996) by a continuous melting and continuous flow set-up. The technical resolution of the NH_4^+ and Ca^{2+} profiles is 2 mm, while the effective resolution is 3-4 cm. Two methods have been applied to the raw Ca^{2+} data to extract as much information as possible from these data. One set has been deconvoluted to account for mixing in the apparatus during measurements. Another variant of the Ca^{2+} data has also been created, by high-pass filtering. The long term trends are removed, so that the high-frequency oscillations, which are of interest for annual counting, are enhanced.
The dust and NO_3^- concentrations were measured by Hammer and others (1997) in 1-10 mm resolution on melted ice. The effective resolution of the data is considered to be of 1-4 cm. The dust concentrations were measured by laser and calibrated by a Coulter Counter.

Method

The dating of Bølling-Allerød is performed by counting annual cycles in deconvoluted δD, deconvoluted δ^{18}O, NH_4^+, Ca^{2+} (raw, deconvoluted and high-pass filtered), dust and NO_3^- (Table 1, Figure 2). As seen in Table 1 and Figure 1, the stable isotope data cover less than half of the whole interval. The multi parameter counting is done manually with all the parameters present at one time. One "master" series of years is established from a common interpretation of the cycles seen in all the different series. In Figure 2 this master series can be seen as dots

on the NH_4^+ profile. A “certain year” is stated as an annual cycle which is clearly seen in all (or most) of the parameters. A certain year is symbolised with a black dot. However, sometimes the cycles may be hard to interpret, e.g. that one series indicates a year where another series does not, or that a possible year is seen as a shoulder on a flank of a peak. These ambiguities lead to “uncertain years” (open dots). The best estimate is taken as the certain years + half of the uncertain years. The uncertainty is taken as half of the uncertain years. This uncertainty reflects the degree of difficulty in interpreting the available data, but does not reflect the “true” uncertainty, as there might be a bias in the dating, e.g. if the data does not resolve all the years.

The counting was first performed on the sections where all the data where available (i.e. in the intervals where the stable isotopes have been measured), aiming at finding an overall agreement between the series. Thereafter, the rest of the Bølling-Allerød period was counted, using the experience that was gained from intervals containing stable isotope profiles.

The definition of the onset of Bølling (GI 1e) and the termination of Allerød (GI 1abc) are based on sharp shifts seen in the deuterium excess profile (T. Popp, pers. comm.) in the NorthGRIP ice core (Dahl-Jensen and others, 2002). These dephts are transferred to GRIP-depth by matching profiles of ECM, DEP, Ca^{2+}, NH_4^+ (and $\delta^{18}O$) from the two ice cores (Taylor and others, 1993; Fuhrer and others, 1993, 1996; Johnsen and others, 1997; Dahl-Jensen and others 2002; Röthlisberger and others, 2000; Bigler, 2004; NGRIP members, 2004). Deuterium excess, which reflects the conditions in the source area for the moisture (Merlivat and Jouzel, 1979; Johnsen and others, 1989), is characterised by abrupt shifts at transitions from one climate period to another. Hence, this parameter is useful for defining the onset and terminations of the climate periods. The deuterium excess is not available from the depth of interest in the GRIP core. The definition of the transition between Bølling and Older Dryas and the transition from Older Dryas (GI 1d) to Allerød are defined by using δD and $\delta^{18}O$ in the GRIP ice core. See

Data	*Depth*	*L*	Δx	*D/H*	*BA*
	m	m	m		
δ^{18}O I	1689.61 - 1703.35	13.75	0.01	D	Mid A
δ^{18}O II	1749.01 - 1750.10	1.10	0.01	D	Start B
δD I	1714.35 - 1719.85	5.50	0.01	D	OD
δD II	1729.20 - 1735.25	6.05	0.01	D	Mid B
δD III	1744.6 - 1755.05	10.45	0.01	D	Start B
NO_3^- ♮	1662.4 - 1753.3	90.90	0.001-0.01		BA
Dust ♮	1662.4 - 1753.3	90.90	0.001-0.01		BA
Ca^{2+} †	1662.4 - 1753.3	90.90	0.002	D+H	BA
NH_4^+ †	1662.4 - 1753.3	90.90	0.002		BA

♮ Hammer and others, 1997; Hammer, in press.

† Fuhrer and others, 1993, 1996.

Table 1. The table displays the depth intervals of the data from the GRIP ice core used for annual counting of Bølling-Allerød. The length of each data interval is shown in the column marked L, while Δx is the sample interval of the data series. Data that have been deconvoluted or high-pass filtered are marked with D or H. The column BA indicates which part of Bølling (B), Older Dryas (OD) or Allerød (A) the series cover. The depths 1753.3 m and 1662.4 m are taken as the onset of Bølling and the termination of Allerød, respectively. The depth interval of Older Dryas is defined to be 1715.0 - 1718.6 m. See text for explanation.

Table 1 for these depths. The depths of the onset of Bølling and the termination of Allerød differ slightly from those defined in (Johnsen and others, 1992), which were based on ECM and from those defined by Hammer (in press) and Hammer and others (1997), however, the depths of Older Dryas were not stated in any of those papers.

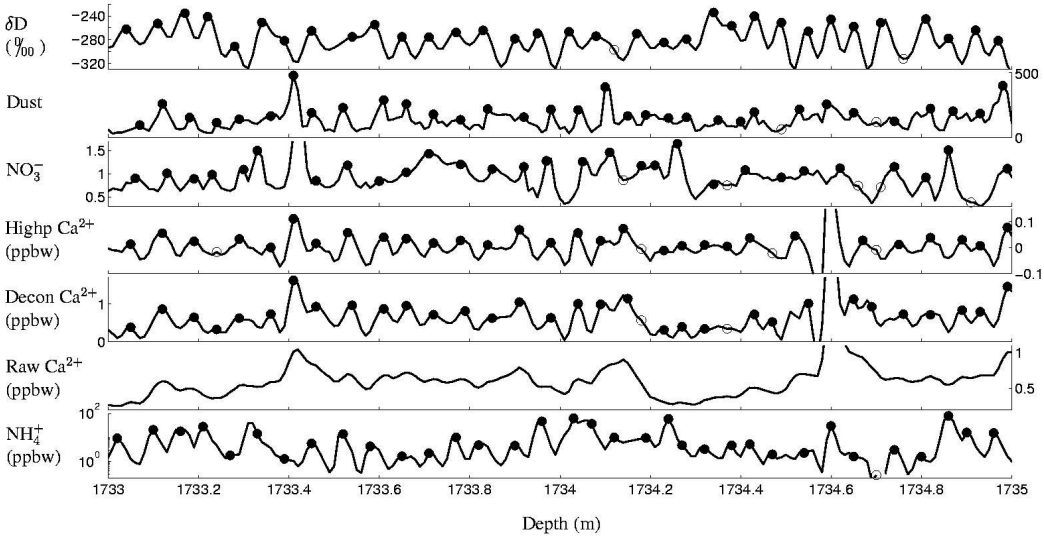

Fig.2. Multi parameter dating. Counting of annual layers is performed on deconvoluted δD (or $\delta^{18}O$), dust, NO_3^-, Ca^{2+} (high-pass, deconvoluted and raw) and NH_4^+. Black dots represent certain annual layers, whereas open dots indicate uncertain annual layers. All the series are given the same amount of dots, based on a common interpretation of the cycles in the different parameters. The dots on the NH_4^+ profile constitute the "master" series. Regarding the Ca^{2+} series, the dots are put on the deconvoluted and high-pass filtered data only, but the interpretation is based on all the three Ca^{2+} variants. The units on the dust and NO_3^- profiles are arbitrary.

Results

Figure 3 and 4 show all the intervals of the new high-resolution stable isotope data from Bølling-Allerød in the GRIP ice core. The δ-values are relative to the VSMOW-SLAP scale. In Figure 3 the raw and deconvoluted data are plotted together. The intervals are labelled δD Interval I, δD Interval II and δD Interval III, δ^{18}O Interval I and δ^{18}O Interval II, according to Table 1. The stable isotope profiles cover a total depth of 36.85m, of which 1.1m is an overlap between δ^{18}O

Interval II and a part of δD Interval III. This overlapping section is displayed in Figure 4, where the raw data are plotted in the upper panel and the deconvoluted data are shown in the lower panel. The overlapping δD and δ^{18}O series are from two different cuttings of the ice and they were measured separately.

Figure 5 displays the MEM power spectra for δ^{18}O Interval II and for the section of δD Interval III that overlaps with the δ^{18}O data. The spectral densities of the δ^{18}O profile have been multiplied with 64 to facilitate the comparison with the spectral densities of the δD section. The power spectra of the raw data (thick lines) show how the amplitudes of high frequencies have been diminished by the diffusion in the firn and ice. The spectral densities in the high frequency domain have been lowered, so that they are indistinguishable from the nearly flat level (white noise) that represents the measuring error (see Table 2). The arrow indicates what is considered as the annual peaks in the power spectra. Both of the spectra for the raw data reveal an annual peak around 14-19 cycles per meter, which corresponds to a layer thickness of 5-7 cm. It is noticed that the annual peak is not very pronounced and that it is situated close to the noise level and therefore close to the cut-off frequency. By comparing the spectra of the raw δD and δ^{18}O in a band around the annual peak, it is observed that the power of δD is higher than for δ^{18}O, relative to that at lower frequencies. This means that the annual signal of the δD has experienced less damping compared to the annual signal in the δ^{18}O. The thin lines in Figure 5 are the power spectra of the back-diffused series. These spectra show how all the frequencies below a certain limit (determined by the cut-off frequency) are amplified to correct for the diffusion. The power density of the annual cycle, which is of interest for dating, has been increased. Table 2 lists specifications on parameters that have been used in the MEM spectral analysis and deconvolution of the stable isotope data. The diffusion length σ and the cut-off frequency f_{max} are used for the inverse transfer function $\exp(0.5 \cdot k^2 \cdot \sigma^2)$, where $k = 2\pi \cdot f$ is the wave number. The choice of cut-off frequency is a best compromise between excluding the noise at higher frequencies and including the annual peak. A f_{max} of $\sim$20 cycles m^{-1} seems to fulfil these conditions for the stable isotope profiles in Bølling-Allerød. This means that back-diffused data are capa-

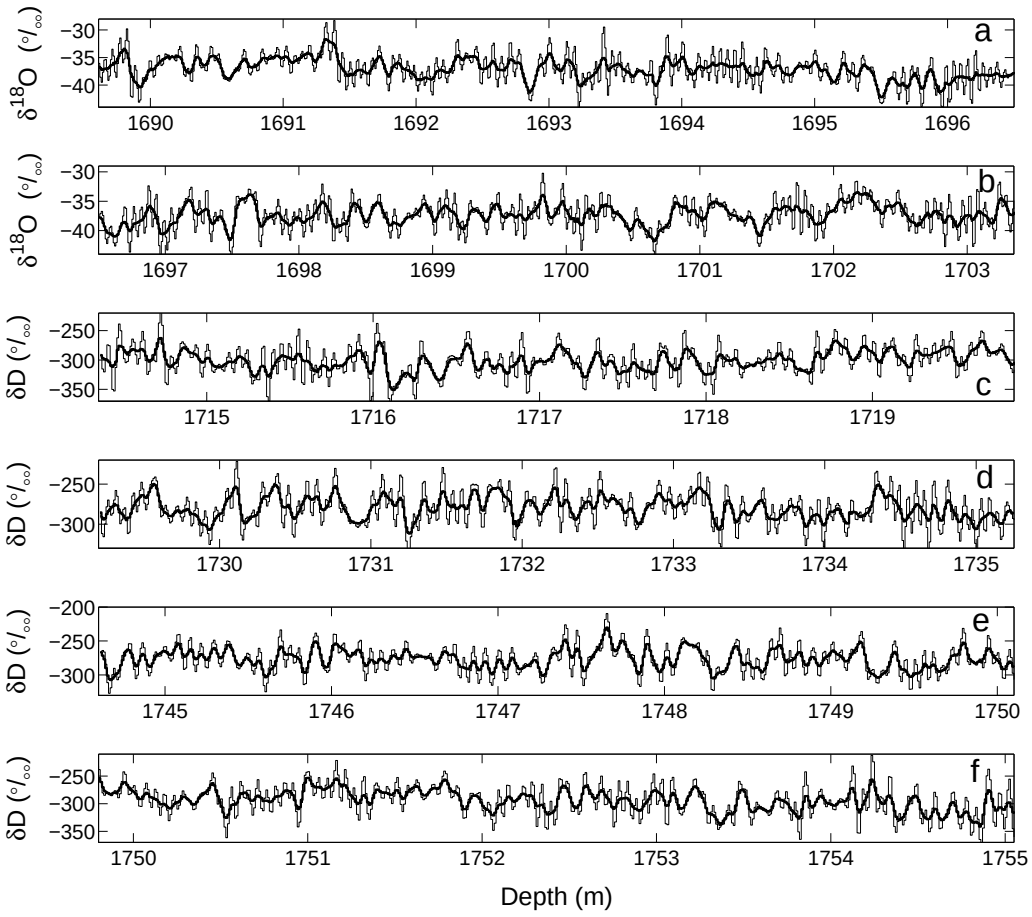

Fig.3. Intervals of high-resolution isotope profiles from Bølling-Allerød in the GRIP ice core. Thick lines = measured data. Thin lines = deconvoluted data where the initial isotope profile has been reconstructed (back-diffusion). The reconstructed annual signal is used for dating by counting summer peaks of high isotope values. Please note that the depth scales on the panels are different. All δ-values are relative to the VSMOW-SLAP scale. (a,b) $\delta^{18}O$ Interval I, (c) δD Interval I, (d) δD Interval II and (e,f) δD Interval III. See Figure 4 for $\delta^{18}O$ Interval II.

ble of resolving annual layers of a thickness $\geq$5 cm. The power spectra shown in Figure 5 are typical for all the isotope intervals, although the annual peak gets

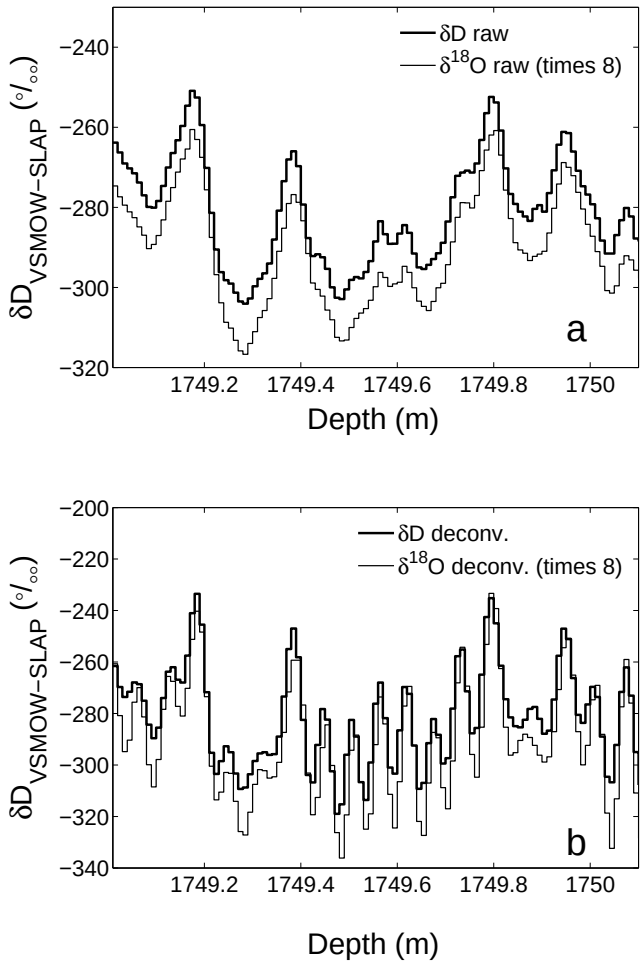

Fig.4. δD and $\delta^{18}O$ in the overlapping section in early Bølling. (a) Raw data. (b) Back-diffused data. Thick lines = δD from a part of δD Interval III. Thin lines = $\delta^{18}O$ Interval II. The $\delta^{18}O$-values are multiplied by 8. There is good agreement between the two different isotope profiles, which were measured separately on different cuttings of the ice.

more blurred out for the longer intervals such as δ^{18}O Interval I in Allerød, where the variability in the layer thickness is likely to be higher, due to the presence of more climatic shifts.

One set of the Ca^{2+} data was deconvoluted to correct for mixing in the appa-

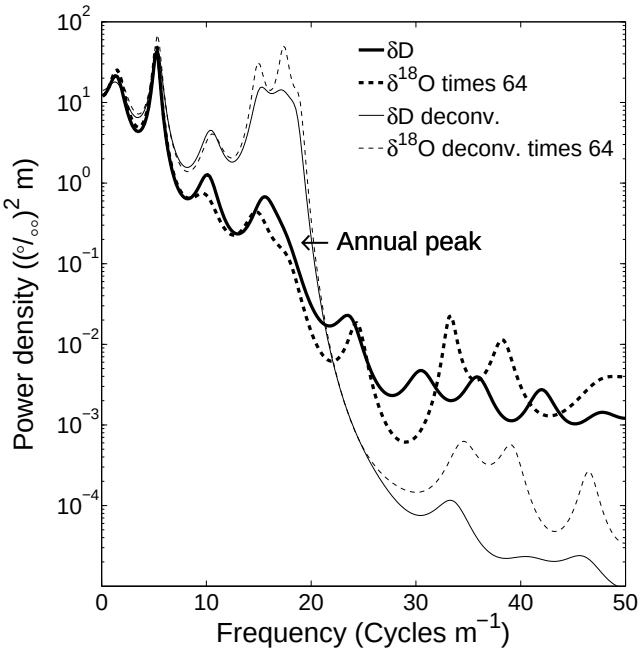

Fig.5. MEM spectral densities for $\delta^{18}O$ Interval II (dotted lines) and a part of δD Interval III (solid lines) in the overlapping section in early Bølling (see Figure 4). Thick lines = Raw data. Thin lines = Back-diffused data. Autoregressive order m is 20, f_{max} is 19 and σ is 0.0185 m (δD) and 0.021 m ($\delta^{18}O$). The annual peak is seen around 14-19 cycles per meter, which equals an annual layer thickness of 5-7 cm. The spectral densities of $\delta^{18}O$ are multiplied with 64 to make the comparison with the spectral densities of δD easier. For wave numbers around the annual peak the damping is smaller for δD than for $\delta^{18}O$.

ratus. The transfer function was $\exp(0.1 \cdot f)$, where f is frequency. The cut-off frequency was 30 cycles m^{-1}, thus the data are able to resolve years of a thickness down to 3.3 cm. It should be mentioned that the deconvolution corrects only the amplitudes of the cycles, not their relative phases. Another set of Ca^{2+} was filtered through a smooth Gaussian high-pass filter.

When looking at the seasonal cycles in all the parameters (an example is seen in Figure 2) it is seen that there is an overall agreement between the parameters.

Interval	σ	m	f_{max}	*Meas. error*
	m		m^{-1}	$‰$
δD I	0.021	30	20	0.9
δD II	0.0215	30	19	0.75
δD III	0.0185	30	21	0.55
δ^{18}O I	0.023	40	19	0.1
δ^{18}O II	0.021	20	19	0.085

Table 2. Parameters used in MEM spectral analysis. σ is diffusion length in meter, m is autoregressive order and f_{max} is the maximum frequency which is allowed in the back-diffusion. The measuring error is the accuracy of the reported δD and δ^{18}O values. The filter length was 100 points. The mean of each of the data series is preserved during the deconvolution process.

NO_3^- is the parameter that is the most deviating, generally showing less cycles than the other parameters. However, in periods NO_3^- agrees well with the other parameters. The dust profile often have more peaks than the other parameters. Under present day conditions NH_4^+ and NO_3^- have maxima during summer like δD and δ^{18}O, while dust and Ca^{2+} normally peak during spring. This is also the main feature during Bølling-Allerød, though there are periods where this is not the case. The parameters are often out of their usual phasing, especially in Allerød. Hence, the seasonality pattern seems to have had a higher variability than for present day conditions.

The depth scales of dust and NO_3^-, which were measured simultaneously, have been shifted a few places within the interval of investigation. This is done because of indications of holes in data or discrepancies in the depth of characteristic peaks observed both in Ca^{2+} and dust. The adjustment of the depth scales was aiming at synchronising these distinct peaks, under the assumption that characteristic peaks in Ca^{2+} and dust reflect the same deposition events. The range of shift was be-

tween -70 mm to +50 mm, where the latter amount of displacement was the most common.

The annual layer counting based on seasonal variations in δD, δ^{18}O, NH_4^+, Ca^{2+} dust and NO_3^- gives an estimated length of Bølling of 586$\pm$17 years, a length of 70$\pm$4 years for Older Dryas and a length of Allerød of 971$\pm$31 years. The uncertainty reflects the inconsistency between the series and the difficulty of interpreting the peaks and shoulders. The uncertainty does not take into account for any bias in the counting. The corresponding mean annual layer thickness of the three periods are 5.9 cm, 5.1 cm and 5.4 cm.

Discussion

The method of counting has been based on a common interpretation of all the data series, first in the intervals containing stable isotopes and then in the rest of the Bølling-Allerød period. The result is highly dependent on the resolution and the internal consistency of the data series. The dust profile generally have more peaks than the other parameters, advocating for the highest number of years, while the stable isotopes and the NO_3^- generally put a lower limit on the number. The Ca^{2+} and NH_4^+ generally serve as good dating tools. The effective resolution of these profiles is 3-4 cm, so they are able to resolve cycles up to this wave length. As previously mentioned, dust can have more than one peak within some years. The exclusion of dust peaks which are considered as “double peaks” has been decided by comparison with the seasonal cycles in the stable isotopes, Ca^{2+}, NH_4^+ and NO_3^-. Hence, it is crucial that these parameters can resolve all the years. Within certain periods this is definitely not the case for NO_3^-, because the profile is too smooth. Within these intervals, no weight has been put on the NO_3^- in the interpretation. When it comes to δD and δ^{18}O, it is evident that the annual cycles are present in the stable isotope profiles from this interstadial. The power spectra reveal a peak around 14-19 cycles m^{-1} for both δD and δ^{18}O, which indicates that

there is power left in the annual signal in both of the stable isotope series, and that they can be used for dating purposes. That this peak reflects a true seasonal signal, is confirmed when seeing the good agreement between δD and δ^{18}O in the overlapping section in Figure 4. If the peaks in the spectral densities were representing noise only, it would not be possible to create such a compelling agreement between the back-diffused δD and δ^{18}O data, as the noise in the two profiles is uncorrelated. Hence, it is unquestionable that there is power left in the annual amplitude of the stable isotope profiles. What remains to be answered is, if all the years are resolved. The method of using stable isotopes for dating is certainly at the limit at this depth, where the ice is 14-15 kyr old. The MEM power spectra of the raw data show that there is little power left in the annual cycle and that the annual peak is close to the noise level. This indicates that some years of low accumulation (high frequency) may not have been revealed by the deconvolution, as they are hidden in the noise and thereby ruled out by the cut-off frequency. With a cut-off frequency of $\sim$20 cycles m^{-1}, annual layers with a thickness less than $\sim$5 cm will not be resolved. This is supported by the fact that shoulders are seen on flanks of δ-peaks when other parameters have peaks (or clear shoulders). If some years are lost in the stable isotope profiles this will lead to a too low estimation of the duration of the periods.

In the section where the δD and the δ^{18}O profiles overlap, it is observed that the damping of the signal is stronger for δ^{18}O than for δD. This is due to less diffusion of molecules containing ^{2}H compared to molecules containing ^{18}O and is in accordance with earlier results and theory (Johnsen and others, 2000). The lower damping of the δD signal suggests that δD is slightly better for dating when working with ice where the amplitude of the annual signal of the stable isotopes is close to the limit of detection.

According to data from Dahl-Jensen and others (1993) the mean accumulation rate (based on δ^{18}O) at GRIP in Bølling was 0.23$\pm$0.02 myr^{-1}, while it was 0.15$\pm$0.02 myr^{-1} in Older Dryas and 0.18$\pm$0.02 myr^{-1} in Allerød. As 0.20 myr^{-1}

is considered as the minimum accumulation rate under present day conditions for the annual cycle to survive (Johnsen, 1977), it is interesting that it is possible to detect the annual amplitude within the stable isotope series from Older Dryas and Allerød. This can either be explained by higher accumulation rates than those derived from δ^{18}O, or by lower temperatures compared to present. δ^{18}O derived paleotemperatures (Johnsen and others, 1995) from the GRIP ice core shows that it was only 1 $^{\circ}$ C colder during Bølling compared to today, while it was 5-12 $^{\circ}$ C colder during Older Dryas and Allerød. Lower temperatures may have slowed down the process of diffusion in the firn and ice.

Compared to the Bølling interval, the data in Older Dryas and Allerød are more difficult to interpret. The seasonal variability is higher, the parameters are often out of phase and the agreement between the data is less compelling. The mean annual layer thickness in Bølling agrees well with the findings of Dahl-Jensen and others (1993), where the mean annual layer thickness in this period was found to be 5.8$\pm$0.6 cm. However, the mean annual layer thickness within Older Dryas and Allerød are greater than those found by Dahl-Jensen and others (1993). Their estimates of the mean annual layer thickness is 4.0$\pm$0.3 cm and 4.9$\pm$0.7 cm in Older Dryas and Allerød, respectively, with minima between 3-3.5 cm. This could indicate that some of the annual layers within Older Dryas and Allerød are too thin to be resolved properly by the data used in the multi parameter dating.

Table 3 displays other estimates of the duration of the Bølling, Older Dryas and Allerød periods in Greenlandic ice cores. When comparing with the previous stratigraphical dating on the GRIP ice core (Hammer and others, 1997; Hammer, in press), it is seen that the number of years is substantially lower for the multi parameter approach. The Older Dryas was not specified in the work by Hammers and others and their definitions of the onset and terminations differed slightly from those used in this study (see Table 1 and 3). By using their depths, the corresponding estimates for the multi parameter approach are the following: Bølling: 585$\pm$17 and Allerød: 1028$\pm$34. These estimates are $\sim$20% and $\sim$30% shorter

Core	*Method*	*B*	*OD*	*A*
		yr	yr	yr
GRIP	Ca^{2+}, NH_4^+, dust, δD, δ^{18}O, NO_3^-	586±17	70±4	971±31
GRIP	Dust †	736		1432
GRIP	Modelled (ss09sea)♭	643	92	1167
GISP2	Ice layer count ‡	580	80	1120
NGRIP	CFA-data ♮	613±16	93±1	1090±29

† Hammer and others, 1997; Hammer, in press.

♭ Johnsen and others, 2001.

‡ Stuiver and others, 1995; Meese and others, 1997; Alley and others, 1997

♮ NGRIP dating group, pers. com.; S. O. Rasmussen and others, in prep.; R¨othlisberger and others, 2000; Bigler, 2004.

Notes: Older Dryas were not specified in Hammer and others (1997) or Hammer (in press). Their depths used for defining Bølling and Allerød are 1572.85 m, 1718.20 m and 1662.65 m. The uncertainty on the GISP2 dating is 5% (Alley and others, 1993). Depths used in the GISP2 dating for defining the periods have not been accurately transferred to the GRIP scale, but comparison of the δ^{18}O profiles from GRIP (Johnsen and others, 1997) and GISP2 (Stuiver and others, 1995; The Greenland Summit Ice Cores CD-ROM, 1997) shows that any deviation of the definitions of the onsets and terminations is not of significance compared to the uncertainty in dating. The estimates from the NorthGRIP layer counting are initial results of ongoing work.

Table 3. Estimates of the duration of Bølling (B), Older Dryas (OD) and Allerød (A) from Greenlandic ice cores. The GISP2 (Greenland Ice Sheet Project Two) ice core (Grootes and others, 1993) is situated 28 km W of GRIP and the NorthGRIP ice core (Dahl-Jensen and others, 2002) is located 325 km NW of GRIP.

than those found by Hammer and others. This huge deviation can be explained by the different ways of approaching the layer counting. The dating accomplished by using dust concentrations only, without guidance from other parameters, may

have overestimated the number of years, by including too many "double peaks". On the other hand, the method that has been used in this study, may have underestimated the duration of the climate periods, as the "restricting" data are not able to resolve annual layers of low thickness, especially in colder parts of the periods, where the accumulation rates have been lower. Compared to the modelled time scale ss09sea (Johnsen and others, 2001), which is based on a Dansgaard-Johnsen flow model and δ^{18}O-derived accumulation rates, it is seen that the new estimates from the multi parameter counting are $\sim$9%, $\sim$24% and $\sim$17% shorter, for Bølling, Older Dryas and Allerød, respectively.

The estimate of the length of Bølling agrees well with the number of years found by annual layer counting of the GISP2 ice core (Alley and others, 1993, 1997; Stuiver and others, 1995; Meese and others, 1997). The estimated durations of Older Dryas and Allerød are $\sim$13% shorter than those from the GISP2 layer counting.

The NorthGRIP ice core (Dahl-Jensen and others, 2002; NGRIP members, 2004) is currently being dated by the members of the NorthGRIP dating group (pers. com.). The stratigraphical dating of this core is made by identification and counting of annual cycles as observed in chemical components measured in a continuous flow system (Röthlisberger and others, 2000; Bigler, 2004). By comparing with preliminary results from the ongoing dating of the NorthGRIP core (S.O. Rasmussen and others, in prep.), it is seen that the present estimate of the duration of Bølling is within 2 σ of the initial estimate of the length of Bølling in the NorthGRIP core. The estimated durations of Older Dryas and Allerød are $\sim$25% and $\sim$11% shorter than those from the dating of the NorthGRIP core.

To summarize, the durations of Bølling-Allerød, estimated by multi parameter layer counting in the GRIP ice core, are generally shorter than other estimates from ice cores in the same region. The estimate of the Bølling period agrees well with GISP2 annual layer counting and with the initial results from the NorthGRIP stratigraphical dating, while the estimates of Older Dryas and Allerød are significantly shorter compared to the other datings seen in Table 3. This indicates that the data used in the multi parameter approach in the GRIP core are able to resolve annual layers in the relatively warm Bølling, while some years may have been lost

in the colder Older Dryas and Allerød.

Conclusion

Multi parameter counting has been accomplished in the Bølling-Allerød period (Greenland Interstadial 1) in the GRIP ice core, by using the parameters Ca^{2+}, NH_4^+, dust, NO_3^- and new stable isotopes profiles showing seasonal variations.
New high-resolution data presented in this study shows that it is possible to use stable isotopes for stratigraphical dating of glacial ice from Greenland Interstadial 1. The annual cycle is seen in MEM power spectra and the cycles of the stable isotopes compare well with the annual cycles in the chemical data series and the seasonal variations in the dust concentrations. It is, however, necessary to deconvolute the measured isotope profiles to reconstruct the initial isotope signals. By this method the annual cycles are amplified and easier to interpret. The maximum resolution of the deconvoluted stable isotope data from Bølling-Allerød is $\sim$5 cm, so annual layers of less thickness will not be resolved by these data. This implies that some years are lost in colder periods having lower accumulation rates, especially within the Older Dryas and the Allerød periods. Furthermore, this study confirms the findings of Johnsen and others (2001) that the damping of the annual amplitude, due to diffusion in the firn and ice, is stronger for δ^{18}O than for δD. This suggests that δD is better suited for dating than δ^{18}O when working on ice where the annual signal in the data is weak.
That the annual amplitudes in the δD and δ^{18}O profiles are detectable, suggests that the annual accumulation rate during the Bølling-Allerød period was at least (or close to) 0.20 m ice per. year. With a lower accumulation rate, it would be less likely that the annual signal would survive the diffusion processes in the firn and ice (Johnsen, 1977).
The estimated durations of the Bølling (GI 1e), Older Dryas (GI 1d) and the Allerød (GI 1abc) periods based on the multi parameter layer counting in the GRIP ice core are 586$\pm$17, 70$\pm$4 and 971$\pm$31 years, respectively. The uncertainties reflect the difficulty of the interpretation of the available data and do not

take into account any bias in the dating. The estimates are considered, as lower limits for these climate periods, as some years may not have been resolved by the data in colder periods with lower accumulation, especially within Older Dryas and Allerød.

This study underlines the importance of having high-resolution data when performing stratigraphical dating of ice cores, and having a variety of independent parameters showing seasonal variations.

Acknowledgements

The authors are indebted to Veijo Pohjola and one anonymous reviewer for helpful review, as well as the scientific editor, Elisabeth Isaksson, for fruitful comments. The authors would also like to thank Trine Ebbensgaard Strømfeldt, Thore Jürgensen and Anita Boas for providing the high resolution $\delta^{18}O$-data, Sune Olander Rasmussen for providing the program Datetool, Copenhagen Ice Core Dating Initiative (funded by the Carlsberg Foundation) and the Glaciology Group at the Niels Bohr Institute, University of Copenhagen. The staff at the AMC ^{14}C Dating Centre, Department of Physics and Astronomy, University of Århus, Denmark is also thanked for helpful assistance during the δD analysis.

B Standards used during δD analysis

Standard	$\delta D_{VSMOW-SLAP}$ [‰]
Instaar FW1	-2.95
GV	-57.69
Kbh-22	-168.80
Instaar WAIS	-204.50
Instaar GW1	-300.90
Summit	-320.32
Dome C	-442.50

Table B.1: δD values of standards when measured relative to VSMOW (0‰) and SLAP (-428.00‰). Control of the standards during analysis has been performed routinely by Jesper Olsen at the AMS-14C Dating Laboratory in Århus.

C Example of a chromatogram

The chromatogram on the next page displays the reference peak and the sample peak for mass 2 (H_2^+) for sample “S5 Kbh-22 4”. The numbers along the x-axis represent the acquisition time in minutes and the the current in per cent of the max value (peak height) in the sample peak is given along the y-axis. The peak height of the mass 2 sample peak is normally in the order of $\sim$10-20 nA. Simultaneously, a chromatogram for mass 3 (HD^+) is produced. The peak height of the mass 3 sample peak is usually in the order of $\sim$0.005-0.01 nA.

D Runs on the CF-IRMS

Period	*Run*	*Samples*	*Std1*	*Std2*
Sep. 02	Grip1	3118-1 - 3119-45	FW1	GW1
	Grip2	3119-46 - 3121-38	DomeC	GW1
	Grip3	3121-39 - 3123-36		GW1
	Grip4	3123-37 - 3125-27	FW1	GW1
Oct. 02	Grip5a	3125-28 - 3126-33	FW1	GW1
	Grip5b	3125-28 - 3126-33	FW1	GW1
	Grip6	3126-34 - 3127-55		GW1
		+ 3145-1 - 3145-31		
	Grip7	3145-32 - 3147-30		GW1
	Dobsina	Other samples		GV
	Grip8	3147-31 - 3149-29		GW1
	Grip9	3149-30 - 3151-28		GW1
	Grip10	3151-29 - 3153-27		GW1
	Grip11	3153-28 - 3155-26		GW1
	Grip12	3155-27 - 3155-55		GW1
		+ 3173-1 - 3174-25		
	Danham2	Other samples	Kbh-22	GV

Table D.1 continues on the next page.

Period	*Run*	*Samples*	*Std1*	*Std2*
Jan. 03		No successful runs		
Feb. 03		No successful runs		
Apr. 03	S6Danham2h	Other samples	Kbh-22	GV
	S7Grip13	3174-26 - 3176-24		GW1
	S8Grip14	3176-25 - 3178-22	FW1	GW1
Nov. 03	S2Grip15	3178-23 - 3180-20	WAIS	Summit
	S3Grip16	3180-21 - 3182-16	WAIS	Summit
	S4Grip17	3182-17 - 3184-14	WAIS	Summit
	S4Grip17b	3182-17 - 3184-14	WAIS	Summit
	S6Grip18	3184-15 - 3186-3	WAIS	Summit
	S7Grip19	3186-4 - 3187-56	WAIS	Summit
	S8Grip20	3187-57 - 3189-54	WAIS	Summit
	S9Grip21	3189-55 - 3191-52	WAIS	Summit
	S10Grip14g	3176-25 - 3178-22	WAIS	Summit
	S11Danham2i	Other samples	Kbh-22	GV
	S12Danham1	Other samples	Kbh-22	GV
	S13Grip22	3191-53 - 3191-55	WAIS	Summit
		+ Repetitions		

Table D.1: Continued from previous page. The table specifi es which samples and standards that were measured in the different runs on the mass spectrometer in at the AMS ^{14}C Dating Centre) in Århus. Only runs that were successful and runs that are relevant for this project are included in the table.

E Recommendations for future δD analysis

The list beneath briefly summarizes some of the experience from the experimental work that may be of interest for future δD measurements at the AMS ^{14}C Dating Centre in Århus or in a laboratory with a similar IRMS system. Some of the following topics are treated in Olsen et al. [In preparation].

- Injection port liner with inner diameter of 3.2 mm and a length of 99 mm is recommended compared to liner with inner diameter of 2.1 mm and length of 69 mm (See Figure E.1). The period of high memory within the δD measurements corresponds to the period where the latter injection port was used.
- An injection volume $\geq 0.4\mu$l to keep a low memory effect.
- $\sim$2 wash cycles of the needle prior to injection.
- Quartz reactor with the longest neck, as the chromium then is located at the hottest part of the oven (See Figure E.2).
- Chemical packing C or D as illustrated in Figure E.2. The chromium powder seems to last longer compared to packing A and B.
- Vial Supelco 24750-U (2 ml, CLR BMV 11mm CR/SR) is recommended compared to Supelco 27531, as the latter does not fit to the auto sampler and may cause damage.

Figure E.1: Two different injector port liners. See text. Photo by Jesper Olsen at the AMS ^{14}C Dating Centre in Århus.

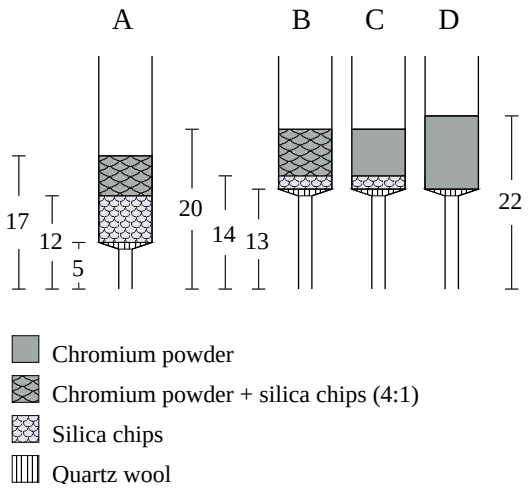

Figure E.2: Chemical packing of the furnace tube in the pyrolysis unit of the elemental analyser. Two different quartz tubes (Transparent Reactor, E12509, o.d. 18-6 mm, Eurovector) were used: One with a 5 cm long neck (left) and one with a 13 cm long neck (right). The diameter of the tube is 18 mm for the upper part and 6 mm for the neck at the bottom. Total length is 45 cm. The lower end of the tube is filled with a thin layer of quartz wool (to avoid the powder from falling out through the neck), silica chips and chromium powder. The amount of the different chemicals were changed (A-D) during the period of measurements. The numbers are in centimetres and refer to the distance from the bottom tip of the tube to the specified height of the chemicals. The drawing is not to scale. Safety precautions was taken during the handling of chromium.

Bibliography

Alley, R., Meese, D., Shuman, C., Gow, A., Taylor, K., Grootes, P., White, J., Ram, M., Waddington, E., Mayewski, P., and Zielinski, G. (1993). Abrupt increase in Greenland snow accumulation at the end of the Younger Dryas event. *Nature*, 362:527–529.

Alley, R., Shuman, C., Meese, D., Gow, A., Taylor, K., Cuffey, K., Fitzpatrick, J., Grootes, P., Zielinski, G., Ram, M., Spinelli, G., and Elder, B. (1997). Visual-stratigraphic dating of the GISP2 ice core: Basis, reproducibility, and application. *Journal of Geophysical Research*, 102:26367–26381.

Andersen, N. (1974). On the calculation of filter coefficients for maximum entropy spectral analyis. *Geophysics*, 39(69-72).

Benson, B. (1962). Stratigraphic studies in the snow and firn of the Greenland ice sheet. *U.S Snow, Ice and Permafrost Research Establishment. Research Report 70*.

Bigler, M. (2004). *Hochauflösende Spurenstoffmessungen an polaren Eisbohrkernen: Glazio-chemische und klimatische Prozessstudien*. PhD thesis, Climate and Environmental Physics, Physics Institute, University of Bern, Switzerland.

Bond, G., Broecker, W., Johnsen, S., McManus, J., Labeyrie, L., Jouzel, J., and Bonani, G. (1993). Correlations between climate records from North Atlantic sediments and Greenland ice. *Nature*, 365:143–147.

Brand, W. A. and Coplen, T. B. (2001). An interlaboratory study to test instrument

performance of hydrogen dual-inlet isotope-ratio mass spectrometers. *Fresenius Journal of Analytical Chemistry*, 370:358–362.

Brooks, P. D., He, S., Dillion, P., and Dawson, T. E. (2004). Drift in the quality control standards using chromium-reactor for D/H analyis of water. Abstract to the Joint European Stable Isotope Users Group Meeting JESUIM 2004, Vienna, International Atomic Energy Agency. http://chemsrv0.pph.univie.ac.at/jesium/abstracts/CH5MET_PO2.PDF.

Coplen, T. B. (1988). Normalization of oxygen and hydrogen isotope data. *Chemical Geology (Isotope Geoscience Section)*, 72:293–297.

Craig, H. (1961). Standard for Reporting Concentrations of Deuterium and Oxygen-18 in Natural Waters. *Science*, New Series 133(3467):1833–1834.

Dahl-Jensen, D., Gundestrup, N. S., Miller, H., Watanabe, O., Johnsen, S. J., Steffensen, J. P., Clausen, H. B., A., S., and Larsen, L. B. (2002). The NorthGRIP deep drilling programme. *Annals of Glaciology*, 35:1–4.

Dahl-Jensen, D., Johnsen, S. J., Hammer, C. U., Clausen, H. B., and Jouzel, J. (1993). Past accumulation rates derived from observed annual layers in the GRIP ice core from Summit, central Greenland. In *Ice in the Climate System*, pages 517–532. Springer-Verlag, Berlin Heidelberg, Germany.

Dansgaard, W. (1964). Stable isotopes in precipitation. *Tellus*, 16:436–468.

Dansgaard, W., Johnsen, S. J., Clausen, H. B., and Gundestrup, N. (1973). Stable isotope glaciology. *Meddelelser om Grønland*, 197(2):1–53.

Donelly, T., Waldron, S., Tait, A., Dougans, J., and Bearhop, S. (2001). Hydrogen isotope analysis of natural abundance and deuterium-enriched waters by reduction over chromium on-line to a dynamic dual inlet isotope-ratio mass spectrometer. *Rapid Communications in Mass Spectrometry*, 15:1297–1303.

Epstein, S. and Sharp, R. P. (1959). Oxygen isotope studies. *Transactions. American Geophysical Union*, 1:81–84.

Fisher, D. A., Reeh, N., and Clausen, H. B. (1985). Stratigraphic noise in time series derived from ice cores. *Annals of Glaciology.*, 7:76–83.

Fuhrer, K., Neftel, A., Anklin, M., and Maggi, V. (1993). Continuous measurements of hydrogen peroxide, formaldehyde, calcium and ammonium concentrations along the new GRIP ice core from Summit, central Greenland. *Atmospheric Environment*, A(27 (12)):1873–1880.

Fuhrer, K., Neftel, A., Anklin, M., Staffelbach, T., and Legrand, M. (1996). High resolution ammonium ice core record covering a complete climatic cycle. *Journal of Geophysical Research*, 101:4147–4164.

Gonfiantini, R. (1978). Standards for Stable Isotope Measurements in Natural Compounds. *Nature*, 271(5645):534.

GRIP Members (1993). Climate instability during the last interglacial period recorded in the GRIP ice core. *Nature*, 364:203-207.

Grootes, P., Stuiver, M., White, J. W. C., Johnsen, S. J., and Jouzel, J. (1993). Comparison of oxygen isotope records from the GISP2 and GRIP Greenland ice cores. *Nature*, 366:552–554.

Hammer, C. U. (In press). Ice core chronology. In *Glaciers and Earth's Changing Environment*, Blackwell Publishing.

Hammer, C. U., Andersen, K. K., Clausen, H. B., Dahl-Jensen, D., Schott-Hvidberg, C., and Iversen, P. (1997). Report on the stratigraphic dating of the GRIP ice core. Special report of the Geophysical Department, Niels Bohr Institute for Astronomy, Physics and Geophysics, University of Copenhagen.

Hammer, C. U., Clausen, H. B., Dansgaard, W., Gundestrup, N., Johnsen, S. J., and Reeh, N. (1978). Dating of Greenland ice cores by flow models, isotopes, volcanic debris, and continental dust. *Journal of Glaciology*, 20(82):3–26.

Herron, M. M. and Langway Jr., C. C. (1980). Firn densification: An empirical model. *Journal of Glaciology*, 25(93):373–385.

IUPAC (1994). Atomic weights of the elements 1993. *Pure and Applied Chemistry*, 66(12):2423–2444.

Johnsen, S. (1977). Stable isotope homogenization of polar firn and ice. In *Proceedings of the Grenoble Symposium on Isotopes and Impurities in Snow and Ice, Grenoble, Aug./Sep. 1975*, IAHS Publ. No. 118, pages 210–219.

Johnsen, S., Clausen, H., Cuffey, K., Hoffmann, G., Schwander, J., and Creyts, T. (2000). Diffusion of stable isotopes in polar firn and ice: the isotope effect in firn diffusion. *Physics of Ice Core Records*, pages 121–140. Hokkaido University Press, Sapporo.

Johnsen, S., Clausen, H., Dansgaard, W., Fuhrer, K., Gundestrup, N., Hammer, C. U., Iversen, P., Steffensen, J. P., Jouzel, J., and Stauffer, B. (1992a). Irregular glacial interstadials recorded in a new Greenland ice core. *Nature*, 359(6393):311–313.

Johnsen, S., Clausen, H., Dansgaard, W., Gundestrup, N., Hammer, C., Andersen, U., Andersen, K., Hvidberg, C., Dahl-Jensen, D., Steffensen, J., Shoji, H., Sveinbjörnsdóttir, A., White, J., Jouzel, J., and Fisher, D. (1997). The δ^{18}O record along the Greenland Ice Core Project deep ice core and the problem of possible Eemian climatic instability. *Journal of Geophysical Research*.

Johnsen, S., Dahl-Jensen, D., Gundestrup, N., Steffensen, J., Clausen, H., Miller, H., Masson-Delmotte, V., Sveinbjörnsdóttir, A., and White, J. (2001). Oxygen isotope and palaeotemperature records from six Greenland ice-core stations: Camp Century, Dye-3, GRIP, GISP2, Renland and NorthGRIP. *Journal of Quaternary Science*, 16(4):299–307.

Johnsen, S., Dansgaard, W., Clausen, H. B., and Langway Jr., C. C. (1972). Oxygen isotope profiles through the Antarctic and Greenland ice sheets. *Nature*, 235:429–434.

Johnsen, S. J., Clausen, H. B., Dansgaard, W., Gundestrup, N. S., Hansson, M., Jonsson, P., Steffensen, J. P., and Sveinbjörnsdóttir, A. E. (1992b). A ”deep”

ice core from East Greenland. *Meddelelser om Grønland Geoscience*, 29, 22 pp.

Johnsen, S. J., Clausen, H. B., Jouzel, J., Schwander, J., Sveinbjörnsdóttir, A. E., and White, J. (1999). Stable Isotope Records from Greenland Deep Ice Cores: The Climate Signal and the Role of Diffusion. *NATO ASI Series*, 1(56). *Ice Physics and the Natural Environment.* Edited by Wettlaufer, J.S., Dash, J.G. and Untersteiner, N.

Johnsen, S. J., Dahl-Jensen, D., Dansgaard, W., and Gundestrup, N. S. (1995). Greenland palaeotemperatures derived from GRIP bore hole temperature and ice core isotope profiles. *Tellus*, 47B:624–629.

Johnsen, S. J., Dansgaard, W., and White, J. W. C. (1989). The origin of Arctic precipitation under present and glacial conditions. *Tellus*, 41 B:425–468.

Langway Jr., C. C. (1967). Stratigraphic analysis of a deep ice core from Greenland. *Cold Regions Research and Engineering Laboratory, Research Report*, 77:1–130.

Meese, D., Gow, A., Alley, R., Zielinski, G., Grootes, P., Ram, M., Taylor, K., Mayewski, P., and Bolzan, J. (1997). The Greenland Ice Sheet Project 2 depth-age scale: Methods and results. *Journal of Geophysical Research*, 102:26411–26423.

Meijer, H. A. J. (2001). Isotope ratio analysis on water: A critical look at developments. In *New approaches for stable isotope ratio measurements. Proceedings of an Advisory Group meeting held in Vienna, 20-23 September 1999*, pages 105–112. International Atomic Energy Agency (IAEA).

Merlivat, L. and Jouzel, J. (1979). Global Climatic Interpretation of the Deuterium-Oxygen 18 Relationship for Precipitation. *Journal of Geophysical Research*, 84(C8):5029–5033.

Merren, T. (2000). Application of an Electrostatic Filter for the Measurement of Hydrogen in Continuous Flow Mode IRMS. Technical brief tb4, Micromass, Manchester, UK.

Micromass (No year available). *IsoPrime User's Guide (ml3.5)*. Micromass UK Limited, Atlas Park, Simonsway, Manchester, M22 5PP. Manual for the IsoPrime mass spectrometer with MassLynx 3.5.

Morrison, J., Brockwell, T., Merren, T., Fourel, F., and Philips, A. (2001). On-line High-Precision Stable Hydrogen Isotopic Analyses on Nanolitre Water Samples. *Analytical Chemistry*, 73(15):3570–3575.

Morse, A. D., Wright, I. P., and Pillinger, C. T. (1993). An investigation into the cause of memory effects associated with the conversion of H_2O to H_2 for D/H measurement. *Chemical Geology (Isotope Geoscience Section)*, 107:147–158.

Mortensen, A. K., Bigler, M., Grönvold, K., Davies, S. M., Johnsen, S. J., and Steffensen, J. P. (In preparation). Tephrostratigraphic correlation of two Greenland ice cores within the Last Termination.

Mortensen, A. K., Bigler, M., Grönvold, K., Steffensen, J. P., and Johnsen, S. J. (2005). Ash layers from the Last Glacial Termination in the NGRIP ice core. *Journal of Quaternary Science*, 20(3):209–219.

Nelson, S. and Dettman, D. (2001). Improving hydrogen isotope measurements for on-line chromium reduction systems. *Rapid Communications in Mass Spectrometry*, 15:2301–2306.

Nelson, S. T. (2000). A simple, practical methodology for routine VSMOW/SLAP normalization of water samples analyzed by continuous flow methods. *Rapid Communications in Mass Spectrometry*, 14:1044–1046.

Nier, A. (1947). A Mass Spectrometer for Isotope and Gas Analysis. *The Review of Scientific Instruments*, 18(6):398–411.

Olsen, J., Seierstad, I., Vinther, B., Johnsen, S., and Heinemeier, J. (In preparation). Memory effects in δD-analysis on a CF-IRMS system.

Platzner, I. T., Habfast, K., Waler, A. J., and Goetz, A. (1997). *Modern Isotope Ratio Mass Spectrometry*, volume 145 of *Chemical Analyis. A series of monographs on analytical chemistry and its applications*. John Wiley & Sons Ltd, England.

Rasmussen, S. O., Andersen, K. K., Svensson, A. M., Steffensen, J. P., Vinther, B. M., Clausen, H. B., Andersen, M. L. S., Johnsen, S. J., Larsen, L. B., Bigler, M., Röthlisberger, R., Fischer, H., Goto-Azuma, K., Hansson, M. E., and Ruth, U. (Submitted). A new Greenland ice core chronology for the last glacial termination. *Journal of Geophysical Research*.

Röthlisberger, R., Bigler, M., Hutterli, M., Sommer, S., and Stauffer, B. (2000). Technique for continuous high-resolution analysis of trace substances in firn and ice cores. *Environ. Sci. Technol.*, 34:338.

Seierstad, I. K., Johnsen, S. J., Vinther, B. M., and Olsen, J. (In press). The duration of the Bølling-Allerød period (Greenland Interstadial 1) in the GRIP ice core. *Annals of Glaciology*.

Stuiver, M., Grootes, P., and Braziunas, T. F. (1995). The GISP2 18O climate record of the past 16,500 years and the role of the sun, ocean and volcanoes. *Quaternary Research*, 44:341–354.

Taylor, K., Hammer, C., Alley, R., Clausen, H., Dahl-Jensen, D., Gow, A., Gundestrup, N., Kipfstuhl, J., Moore, J., and Waddington, E. (1993). Electrical conductivity measurements from the GISP2 and GRIP Greenland ice cores. *Nature*, 366:549–552.

The Greenland Summit Ice Cores CD-ROM (1997). http://www.ngdc.noaa.gov/paleo/icecore/greenland/summit/index.html. Available from the National Snow and Ice Data Center, University of Colorado

at Boulder, and the World Data Center-A for Paleoclimatology, National Geophysical Data Center, Boulder, USA.

Vaughn, B., White, J., Delmotte, M., Trolier, M., Cattani, O., and Stievenard, M. (1998). An automated system for hydrogen isotope analysis of water. *Chemical Geology*, 152:309–319.

Werner, R. A. and Brand, W. A. (2001). Referencing strategies and techniques in stable isotope ratio analysis. *Rapid Communications in Mass Spectrometry*, 15:501–519.